Experimental design for the marine ice sheet and ocean model intercomparison project - phase 2 (MISOMIP2)

Jan De Rydt[1,*], Nicolas C. Jourdain[2,*], Yoshihiro Nakayama[3,*], Mathias van Caspel[4,*],
Ralph Timmermann[4,*], Pierre Mathiot[2], Xylar S. Asay-Davis[5], Hélène Seroussi[6], Pierre Dutrieux[7],
Ben Galton-Fenzi[8], David Holland[9], and Ronja Reese[1]

[1]Department of Geography and Environmental Sciences, Northumbria University, Newcastle, UK
[2]Univ. Grenoble Alpes/CNRS/IRD/G-INP, Institut des Géosciences de l'Environnement, Grenoble, France
[3]Institute of Low Temperature Science, Hokkaido University, Sapporo, Japan
[4]Alfred Wegener Institute, Bremerhaven, Germany
[5]Los Alamos National Laboratory, Los Alamos, US
[6]Thayer School of Engineering, Dartmouth College, Hanover, NH, US
[7]British Antarctic Survey, Cambridge ,UK
[8]Australian Antarctic Division, University of Tasmania, Hobart, Australia
[9]Courant Institute of Mathematical Sciences, University of New York, New York, US
[*]These authors contributed equally to this work.

Correspondence: J. De Rydt (jan.rydt@northumbria.ac.uk) and N. C. Jourdain (nicolas.jourdain@univ-grenoble-alpes.fr)

Abstract. The Marine Ice Sheet and Ocean Model Intercomparison Project - phase 2 (MISOMIP2) is a natural progression of previous and ongoing model intercomparison exercises that have focused on the simulation of ice-sheet and ocean processes in Antarctica. The previous exercises motivate the move towards realistic configurations as well as more diverse model parameters and resolutions. The main objective of MISOMIP2 is to investigate the performance of existing ocean and coupled ice-sheet–ocean models in a range of Antarctic environments, through comparisons to observational data. We will assess the status of ice-sheet–ocean modelling as a community and identify common characteristics of models that are best able to capture observed features. As models are highly tuned based on present-day data, we will also compare their sensitivity to prescribed abrupt atmospheric perturbations leading to either very warm or slightly warmer ocean conditions compared to present-day. The approach of MISOMIP2 is to welcome contributions of models as they are, including global and regional configurations, but we request standardised variables and common grids for the outputs. We target the analysis on two specific regions, the Amundsen Sea and the Weddell Sea, since they describe two different ocean environments and have been relatively well observed compared to other areas of Antarctica. An observational "MIPkit" synthesizing existing ocean and ice sheet observations for a common period is provided to evaluate ocean and ice sheet models in these two regions.

Copyright statement. TEXT

1 Introduction

Model intercomparison projects (MIPs) for standalone ice-sheet models with floating ice shelves have been key to understanding what was needed in ice-sheet models to reproduce fast grounding line migrations similar to those observed in West Antarctica (Pattyn, 2018). In particular, MISMIP (Marine Ice Sheet Model Intercomparison Project; Pattyn et al., 2012) and MIS-MIP3D (Pattyn et al., 2013), both conducted with idealized glacier geometries, highlighted the need for high (sub-kilometer)
model resolution at the grounding line and the inclusion of membrane stresses. Recently, MISMIP+ (Asay-Davis et al., 2016) emphasised the improved agreement in model behaviours across a range of model architectures and the important role of ice-sheet sliding laws for a geometry representative of a highly buttressed ice shelf (Cornford et al., 2020). These MIPs have played a crucial role in the development of credible designs for Antarctic Ice Sheet projection frameworks (Nowicki et al., 2016).

The Ice Shelf Ocean Model Intercomparison Project (ISOMIP; Holland et al., 2003; Hunter, 2006) was the first standardised
configuration for stand-alone ocean models with a thermodynamically active ice-shelf cavity with fixed geometry (henceforth called ice-shelf–ocean models). However, ISOMIP has mostly been used as a test case for individual modelling groups (e.g., Losch, 2008; Gwyther et al., 2015; Mathiot et al., 2017). Its successor, ISOMIP+ (Asay-Davis et al., 2016), was implemented more as a coordinated intercomparison with a provided calibration method and common parameters. Results highlighted fundamental differences in simulated melt rates depending on the vertical discretisation and resolution of ocean models (Gwyther
et al., 2020). When all the ocean models used the same physical parameters, the relationship between basal melt and the ocean circulation in the cavity was consistent across models, but the relationship did not hold when models were run with their typical parameter values (Asay-Davis et al., pers. comm.). This illustrates that despite facilitating the interpretation of an intercomparison exercise, the requirement of common set-ups may push the models far from their typical use, making it difficult to generalise the results for realistic configurations. The use of a single ice shelf in ISOMIP+ and the absence of realistic ocean–
sea-ice dynamics over the continental shelf also made it difficult to generalise the melt sensitivity to the large variety of ice shelf geometries in the whole Antarctic region (Jourdain et al., 2020; Burgard et al., 2022). Hence, previous MIPs motivate the move towards realistic configurations and more diverse model parameters and resolutions. One such approach was recently adopted by the Realistic Ice-sheet/ocean State Estimates (RISE) project in which the circum-Antarctic response of basal melting was evaluated against satellite-derived melt estimates in ten circum-Antarctic ice-shelf–ocean models.

The continued development of ice-shelf–ocean models for Antarctica is a crucial step towards improved forecasts of sea-level rise, and to further our understanding of the complex interactions between the ice sheet and other components of the climate system. However, so far, sea level projections have relied heavily on the use of parameterisations of ocean-induced melt rates in stand-alone ice sheet models. These parameterisations were identified as a major source of uncertainty in the Antarctic Ice Sheet projections from the Ice Sheet Model Intercomparison Project for CMIP6 (ISMIP6; Nowicki et al., 2020;
Seroussi et al., 2020; Payne et al., 2021; Seroussi et al., 2023). Since then, comparisons of these parameterisations to ice-shelf–ocean simulations have been used to better calibrate their sensitivity to ocean warming (Burgard et al., 2022; Reese et al., 2023; Jourdain et al., 2022). However, there is currently limited confidence in the validity of such ice-shelf–ocean simulations for several reasons: 1) important biases remain in the thermohaline structure and dynamical state of the ocean, in particular on

the continental shelf, 2) the parameterizations for ice-shelf basal melt used in ocean models is highly tuned and structurally uncertain, 3) no comprehensive comparison between model data and measurements of ocean properties and basal melt has been carried out. As such, the use of ice-shelf–ocean model output to calibrate melt-parameterisations that inform sea-level projections is questionable. A targeted ice-shelf–ocean MIP with a harmonized comparison of model output to available ocean data, would help identify ocean model similarities and differences, as well as better estimate uncertainties.

While melting parameterisations will undoubtedly remain useful due to their low computing cost compared to actual ocean models, they suffer from important biases despite improved calibration and increased complexity (Burgard et al., 2022). Therefore, many groups engaged in the development of coupled ice-sheet–ocean models, i.e., models in which the ice and ocean dynamics evolve together and feed back on each other (Thoma et al., 2015; De Rydt and Gudmundsson, 2016; Seroussi et al., 2017; Timmermann and Goeller, 2017; Goldberg et al., 2018; Favier et al., 2019; Pelle et al., 2021; Zhao et al., 2022; Pelletier et al., 2022; De Rydt and Naughten, 2024; Bett et al., 2023). While this type of coupling is emerging in Earth System Models (Smith et al., 2021; Siahaan et al., 2022; Comeau et al., 2022), there is currently very limited knowledge on the fidelity of simulated interactions. Similarly to the case of standalone ocean models, a targeted MIP for coupled ice-sheet–ocean models would help identify some of these caveats and quantify uncertainties. The first Marine Ice Sheet Ocean Model Intercomparison Project (MISOMIP1; Asay-Davis et al., 2016) was built along the lines of the aforementioned MISMIP+ and ISOMIP+, with a single, idealized ice shelf and no interaction with atmosphere and sea ice. While MISOMIP1 has been useful for generating cohesion within the ocean and ice-sheet modelling communities and for beta-testing individual coupled models (e.g., Favier et al., 2019), progressing towards more diverse and realistic conditions would bring new information on the state of coupled ice-sheet–ocean modelling.

In this paper, we propose a protocol for MISOMIP2, a new coordinated intercomparison project for standalone ocean models representing ice shelf cavities and for coupled ice-sheet–ocean models. While there previously were distinct names for ocean (ISOMIP+) and coupled (MISOMIP1) experiments, we now embed standalone and coupled experiments within a single acronym, MISOMIP2, for the sake of simplicity.

The first objective of MISOMIP2 is to investigate the robustness and biases of ice-shelf–ocean models (ocean models with fixed ice-shelf cavities) and ice-sheet–ocean models (ocean models with dynamically evolving cavities) in a range of Antarctic environments, through comparisons to observational data that capture the range of natural ocean variability. The comparison to observations is not primarily designed to rank individual models, as targeted model tuning and bias compensations may hide poorly represented physical processes. Our aim is rather to assess the status of ice-sheet–ocean modelling as a community and, if possible, to identify common characteristics of models that are best able to capture observed features. For that, we have gathered a set of reprocessed observational products that can be used for MISOMIP2 or for individual model tests and calibrations. The corresponding observational database is referred to as the "MIPkit" in the following. As our objective is to understand differences between complex models, we will generally follow a "come as you are" (CAYA) approach, with no prescription of model domain, resolution, physical parameters and forcing.

Besides hindcast-type reference simulations, MISOMIP2 also includes a small number of perturbation experiments that are designed to deepen our understanding of model responses to a prescribed (large and abrupt) change in atmospheric conditions

and to a prescribed change in cavity geometry. Importantly, we propose idealized perturbations to focus on strong changes over
85 time windows compatible with a range of models of relatively high resolution, and to have model responses that are relatively
easy to interpret. The initial aim of MISOMIP2 is not to build scenario-based coupled ice-sheet–ocean projections, which is
the remit of ISMIP (Nowicki et al., 2016, 2020). The proposed model intercomparison will however contribute to improved
future ice-sheet projections due to better constrained melting and freezing parameterisations, and future climate simulations
with interactive ice sheets thanks to a better understanding of the strengths and limitations of the various coupling approaches.
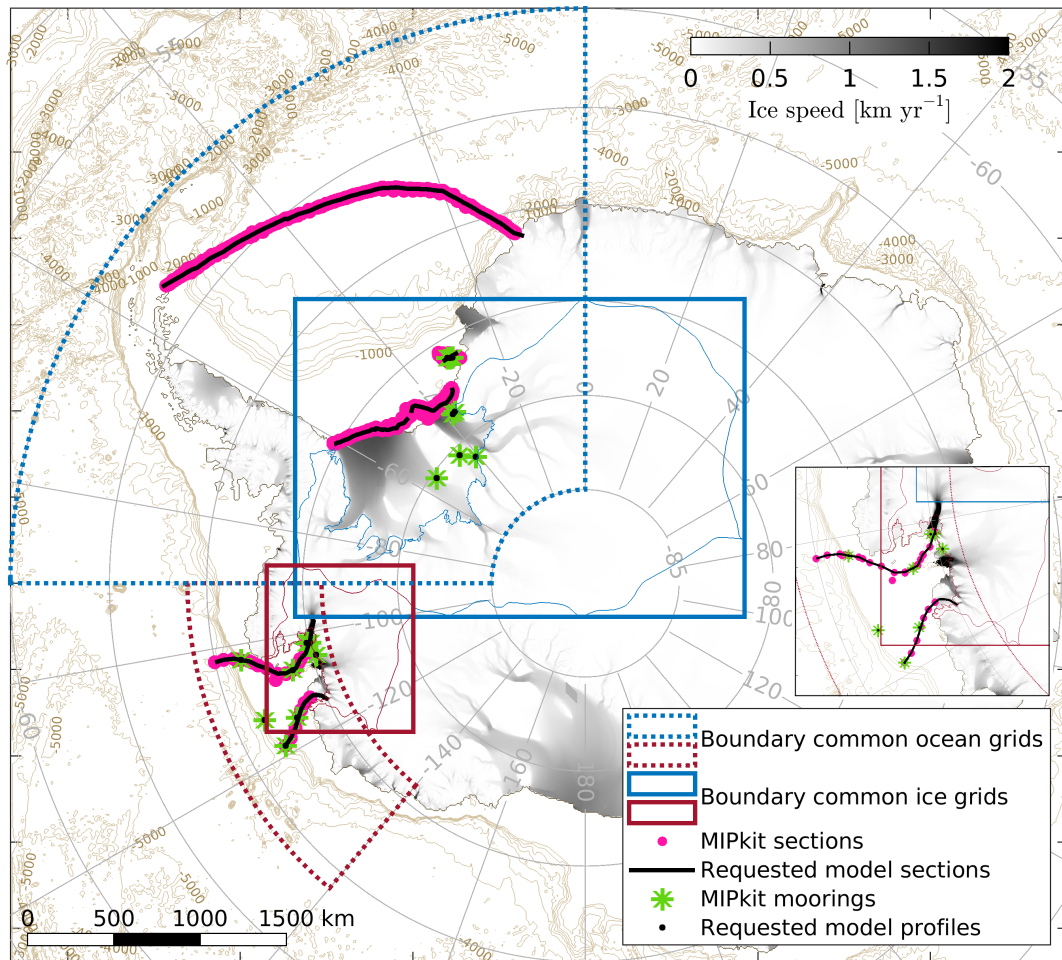

Figure 1. Boundaries of the standard MISOMIP2 grids for the ocean (dashed lines) and ice (solid lines) outputs of the Amundsen Sea (red
lines) and Weddell Sea (blue lines) domains. Black lines indicate the locations of the requested model outputs along vertical sections (two in
the Amundsen Sea, three in the Weddell Sea), as detailed in section 4.1). Geographical locations of the CTD and mooring data provided as
part of the MIPkit are indicated by the green stars and pink dots, respectively. The inset above the legend provides a more detailed overview
of the didfferent section and mooring locations in the Amundsen Sea.

There will be two target regions in MISOMIP2: 1) the Amundsen Sea and 2) the Weddell Sea, and associated ice-sheet drainage basins, as illustrated in Fig. 1. These regions are chosen because they describe two contrasting present-day environments. Deep water masses in the Amundsen Sea are relatively warm, with high ice-shelf basal melt rates driven by Circumpolar Deep Water that is found on the continental shelf (e.g., Jacobs et al., 2013; Dutrieux et al., 2014; Jenkins et al., 2018). The ice-sheet grounding zone has significantly retreated in recent decades (Rignot et al., 2014a; Scheuchl et al., 2016; Milillo et al., 2019, 2022), and there has been significant acceleration and mass loss of the grounded ice sheet in this sector (Rignot et al., 2019; Shepherd et al., 2018). In contrast, the Weddell Sea is relatively cold, with associated low ice-shelf basal melt rates and refreezing beneath some parts of ice shelves due to strong ice-shelf thickness gradients and the presence of High Salinity Shelf Water on the continental shelf (e.g., Nicholls et al., 2009). The Filchner-Ronne Ice Shelf and the upstream ice sheet have remained relatively unchanged over the last decades (Rignot et al., 2019), although future atmospheric perturbations may cause Warm Deep Water intrusions onto the continental shelf, and initiate significant grounding line retreat through enhanced basal melt (Timmermann and Hellmer, 2013; Hellmer et al., 2017; Timmermann and Goeller, 2017; Hazel and Stewart, 2020; Naughten et al., 2021). We would consider a good representation of these very distinct environments in a single configuration (or two analogous configurations of the same model) to be a good indication of model robustness. Moreover, a multi-decadal record of ocean data is available for both regions, with a more comprehensive coverage compared to other parts of the Southern Ocean, which facilities a more in-depth comparison between model results and observations.

In subsequent sections, we describe the experimental protocol for MISOMIP2, including the motivation and description of individual experiments (section 2), a description of the datasets provided in the MIPkit (section 3), and an overview of the requested model outputs (section 4). To illustrate the experimental design, preliminary results from a range of global and regional ocean models and regional ice-sheet configurations are provided.

2 Experiments

2.1 Overview of the MIP experiments

The MISOMIP2 experiments were designed with two broad objectives in mind. First, to test and intercompare the fidelity of ice-shelf–ocean models and ice-sheet–ocean models over the observational period, and second, to assess the sensitivity of models to a plausible change in the shape of the ice-shelf cavities and to a large perturbation in the atmospheric forcing. An overview of the experiments planned in MISOMIP2 and their time windows are provided in Tab. 1 and Fig. 2, respectively. Further details for each experiment are provided hereafter. In all the following, "A" stands for Amundsen, and "W" for Weddell.

- OceanA-hind & OceanW-hind experiments are designed to compare stand-alone ocean model simulations with static ice shelves and *present-day* atmospheric forcing to a common set of ocean observations that are relevant to Antarctic ice shelves, to analyse multi-model sensitivity to external drivers, and to potentially identify clusters of models with a similar behaviour for specific modelling choices.
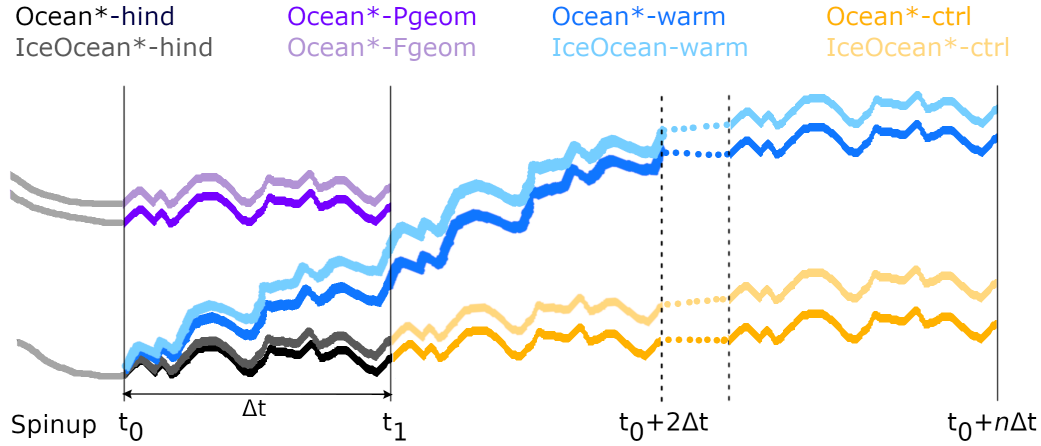
5

Figure 2. Schematic overview of the MISOMIP2 experiments and their respective time windows. As specified in more detail in Section 2, hindcast experiments (black and grey curves) and geometric perturbation experiments (purple curves) will cover the observational period between $t_0 \leq 2007$ and $t_1 \geq 2018$, with the exact time window decided by individual contributors. The atmospheric perturbation experiments (blue curves) and corresponding reference experiments (orange curves) start at time t_0 and end at time $t_0 + n\Delta t$, where $\Delta t = t_1 - t_0$ and n chosen sufficiently large such that melt rates are equilibrated with the atmospheric perturbation (regional models) or $n\Delta t \leq 100$ years (global models).

Experiment name (* is either A or W)	Ocean only (O) or coupled (C)	Atmospheric forcing	Ice-sheet geometry	Time window
Ocean*-hind	O	historical (CAYA)	present-day (CAYA)	$[t_0, t_1]$, with $t_0 \leq 2007, t_1 \geq 2018$
Ocean*-warm	O	historical (CAYA) + prescribed anomaly	present-day (CAYA)	$[t_0, t_0 + n\Delta t]$, with $\Delta t = t_1 - t_0$ and $n\Delta t \approx 100$ yrs
Ocean*-ctrl	O	historical (CAYA)	present-day (CAYA)	$[t_0, t_0 + n\Delta t]$
Ocean*-Pgeom & Ocean*-Fgeom	O	historical (CAYA)	prescribed present (P) and future (F)	$[t_0, t_1]$
IceOcean*-hind	C	historical (CAYA)	time-evolving	$[t_0, t_1]$
IceOcean*-warm	C	historical (CAYA) + prescribed anomaly	time-evolving	$[t_0, t_0 + n\Delta t]$
IceOcean*-ctrl	C	historical (CAYA)	time-evolving	$[t_0, t_0 + n\Delta t]$

Table 1. Overview of the MISOMIP2 experiments, where * is either "A" for the Amundsen domain, or "W" for the Weddell domain. CAYA refers to Come-As-You-Are. Further details are provided in sections 2.1 and 2.2

– OceanA-warm & OceanW-warm experiments are designed to compare the response of simulated melt rates to a transition to *warm* ocean conditions, in response to a rapid modification of the atmospheric forcing. The model configuration is

otherwise identical to the OceanA-hind and OceanW-hind experiments. All models will apply a strong atmospheric perturbation representative of an abrupt shift to a warmer climate in the form of a prescribed anomaly to be added to the present-day forcing used in the OceanA-hind & OceanW-hind experiments. For regional models with open ocean boundaries, an additional temperature and salinity anomaly is provided for the boundaries to represent the ocean warming outside the domain. A detailed description of the perturbations can be found in Sect. 2.3.

- OceanA-ctrl & OceanW-ctrl experiments are extensions of OceanA-hind & OceanW-hind forced by present-day atmospheric conditions to be used as a *control* for the perturbation experiments.

- OceanA-Pgeom/Fgeom & OceanW-Pgeom/Fgeom experiments are designed to compare the response of simulated melt rates in stand-alone ocean models to an imposed modification of the ice-shelf geometry. Two distinct geometries for the Amundsen Sea and Filchner-Ronne cavities are provided: one that represents the *present-day* state of the ice sheet (OceanA-Pgeom and OceanW-Pgeom experiments), and one hypothetical *future* state (OceanA-Fgeom and OceanW-Fgeom experiments). The atmospheric forcing remains unchanged between these experiments. The difference between the OceanA-Pgeom/OceanW-Pgeom and the OceanA-hind/OceanW-hind experiments is that in the former, the present-day geometry of the ice shelves is prescribed and provided as part of the MIPkit (see section 3.3), whereas in the latter the user is free to choose a present-day ice-sheet geometry as part of the CAYA approach. If participants choose to use the Ocean*-Pgeom geometry for their Ocean*-hind experiments, then both experiments will be identical, and results for only one experiment need to be submitted.

- IceOceanA-hind & IceOceanW-hind experiments are similar to OceanA-hind & OceanW-hind focusing on *present-day* conditions, but with coupled ice-sheet–ocean models (including "intermediate-complexity coupling" through parameterisations; e.g., Kreuzer et al., 2021). Here we aim to compare the simulated ice and ocean evolution to recent observations. We will also attempt to estimate the change in bias (if any) that such coupled models attain compared to standalone ocean models.

- IceOceanA-warm & IceOceanW-warm experiments are designed to compare the response of the coupled system to the same idealised *warm* perturbation as for OceanA-warm & OceanW-warm.

- IceOceanA-ctrl & IceOceanW-ctrl experiments are extensions of IceOceanA-hind & IceOceanW-hind over several present-day cycles (in a similar way as in the OMIP protocol Griffies et al., 2016), to be used as *control* for the perturbation experiments. This is used to account for possible drifts in the simulation.

A more detailed description of each experiment, including the aims, type of models, time windows and forcing, are provided in subsequent sections.

Participants are welcome to contribute to any number of experiments, with the only restrictions that 1) results for Ocean*-Fgeom should be accompanied by corresponding results for Ocean*-Pgeom, and 2) results for Ocean*-warm and IceOcean*-warm should be accompanied by corresponding results for Ocean*-ctrl and IceOcean*-ctrl, respectively. We also welcome

7

155 multiple submissions from the same model, e.g. for different parameter configurations or physics, but note that in the analysis of the full MIP ensemble, a weighted approach might have to be applied to avoid a situation where individual models dominate the mean.

2.2 OceanA-hind & OceanW-hind experiments

2.2.1 Aim

160 These experiments will be used to compare multiple ocean simulations to a common set of observations, over the continental shelf and within the ice-shelf cavities. We primarily want to assess the mean state and interannual variability of ocean conditions and simulated sub-ice shelf melt. These experiments will also be used to identify clusters of similar model responses to various modelling choices (e.g., horizontal resolution, vertical grid, atmospheric forcing), and to assess the multi-model response to external drivers (e.g., wind stress variations and surface freshwater fluxes, possibly in relation to large-scale modes of climate 165 variability).

2.2.2 Type of models

Any type of ocean model can be used as long as the original domain includes the main ice shelf cavities, i.e., we are interested in both global and regional configurations. Model contributions to "A" experiments should include at least Pine Island, Thwaites, Crosson and Dotson ice shelf cavities; "W" experiments should include at least Filchner and Ronne ice shelf cavities. We do 170 not impose any further restrictions on the domain size of regional configurations, for example, we do not require models to include the shelf break or the Weddell Gyre. This allows contributions from high-resolution setups with prescribed boundary conditions from larger-scale GCMs.

2.2.3 Time window

All the ocean simulations must be provided after spin up (we let the participants decide on the appropriate duration). All 175 simulations must cover at least 2007-2018, forced by the corresponding atmospheric conditions during that time (i.e., forcing should not be repeated). The proposed time window includes a reasonable amount of observations for both the Amundsen and the Weddell sectors. For the Amundsen Sea, this includes years when a shallow thermocline has been observed (e.g., 2009), and a period when a deep thermocline has been observed (2012–2014). We encourage participants to submit simulations over longer periods if possible, ideally 1979–present, which will be used for model intercomparison and identification of common 180 model biases and variability.

2.2.4 Input/Forcing

Ice-shelf–ocean interactions must be thermodynamically interactive, i.e., ice-shelf basal melt rates are calculated from ocean properties and the corresponding melt water effect is seen by the ocean. For all other modelling choices, we follow a come-as-you-are (CAYA) approach, and we do not define specific requirements for domain size, resolution, bathymetry and ice draft

8

data, sea-ice and ocean model parameters, representation of icebergs if any, data and method to prescribe lateral boundaries, or representation of tidal effects, if any. However, to force the atmosphere-ocean boundary the use of atmospheric reanalysis products with interannual variability is essential, and climatological, normal-year and CMIP forcing are not permitted. The use of a dynamical-thermodynamical sea ice model is recommended, although participants can represent the interannual sea ice variability in a simplified way, if they wish.

The CAYA allows for significant differences in boundary conditions, model architecture and model physics, which might obscure the origin of model biases and feedbacks. At the same time, it can be challenging to analyze results from model configurations that are asked to fit stringent (forcing) criteria. For the ISOMIP+ and MISOMIP1 experiments, for example, this led to model sensitivities that were far away from their default behavior. Moreover, it is unclear what boundary conditions should be imposed, given the spread in model domain size and biases in existing global simulations. MISOMIP2 therefore aims to quantify the inter-model spread and biases for ocean-ice models in their typical configurations. We encourage participants to use the MIPkit data (see section 3) to reduce potential biases and optimize their model setups where possible. While we do not discourage contributions with large biases in present-day ocean conditions, a lower weighting might have to be put on those configurations when analyzing the model sensitivity to anomalies in atmospheric forcing and perturbations in ice-shelf geometry (sections 2.3 and 2.5). We may propose more constrained simulations with a common set of boundary conditions in future iterations of MISOMIP, but this would come at a later stage as the experimental design would benefit from the analysis of the currently-proposed MISOMIP2 experiments.

2.3 OceanA-warm & OceanW-warm experiments

2.3.1 Aim

These experiments will be used to compare the melt response to a transition to warm oceanic conditions resulting from a strong and abrupt perturbation of the atmospheric forcing. As we do not expect all ocean models to reach the same warming levels over the duration of the experiment, the melt response will be considered as a function of regional and/or cavity warming. This will provide a valuable database for evaluating and tuning melt parameterisations used in ice sheet models. We will also identify clusters of ocean responses and attempt to link them to the representation of important physical phenomena (e.g., sea ice production, currents at the shelf break). An example of OceanA-warm & OceanW-warm simulation is shown in Fig. 3.

Note that all contributions to the OceanA-warm and OceanW-warm experiments should be accompanied by corresponding results for the OceanA-ctrl and OceanW-ctrl experiments, as detailed in subsection 2.4.

2.3.2 Type of models

The requirements are similar to OceanA-hind & OceanW-hind. It should be noted that models prescribing energy fluxes at the surface of the ocean rather than calculating fluxes based on a sea-ice model and surface air properties will not be able to run these perturbation experiments. Equally, regional setups that are restricted to a small area of open ocean on the continental shelf are less suitable for this type of experiment, and might be omitted from the analysis.

2.3.3 Time window

Simulations will start from the same initial state and timestamp as the OceanA-hind & OceanW-hind experiments, as illustrated in Fig. 2 and Fig. 3. Experiments will cover the same time window as the OceanA-hind & OceanW-hind simulations, $[t_0, t_1]$, but with a possible extension beyond t_1 to allow ice-shelf melt rates to reach a new quasi steady state. The extended simulations will be forced by cyclically repeating perturbed atmospheric conditions used for the $[t_0, t_1]$ time period, as described in detail below. For example, if the OceanA-hind & OceanW-hind simulations cover the 2000–2019 time window (after a spin up prior to 2000), then OceanA-warm & OceanW-warm simulations should start in 2000 and be forced by 20-year cycles of perturbed 2000–2019 conditions. The number of cycles is to be decided by the participants, and should be chosen such that melt rates reach a quasi steady state under the perturbed conditions. Importantly, we note that for global configurations, the total length of the simulations should not exceed 100 years, even if a steady state is not reached, as slow change of the global thermohaline circulation is not the focus of MISOMIP2.

Note that the time variable will continue forward over the different cycles, e.g., it will indicate 2020–2039 in an extension over a second cycle of the 2000–2019 present-day period.

2.3.4 Atmospheric Input/Forcing

We provide a perturbation that participants are requested to add to their atmospheric forcing used in their OceanA-hind & OceanW-hind experiments. This perturbation was fully described and tested in Mathiot and Jourdain (2023), and key details are provided below. In case of regional configurations, an additional perturbation is to be applied to the ocean and sea-ice lateral boundary conditions, as described in the *Lateral Input/Forcing* paragraph below.

The prescribed atmospheric perturbation consists of a 12-month record (i.e., one entry for each month), with effective timestamps at the middle of each month. The time series is to be added to each year of the OceanA-hind & OceanW-hind forcing, using linear interpolation between the middle of two consecutive months to recreate a continuous perturbation.

The perturbation was extracted from monthly outputs of the IPSL-CM6A-LR projections (Boucher et al., 2020; Lurton et al., 2020) under the SSP5-8.5 emission scenario (Meinshausen et al., 2020). Monthly anomalies from 1975-2014 to 2260-2299 were calculated for all the fields used to calculate the ocean and sea-ice surface boundary conditions (2-m air temperature and specific humidity, 10-m zonal and meridional winds, surface pressure, downward shortwave and longwave radiative fluxes, total precipitation, snowfall). To limit computing cost and focus on regional changes while aiming for a strong change, the perturbation is applied abruptly from the same initial state as OceanA-hind & OceanW-hind, i.e., after a spin-up under present-day forcing (Figure 2).

Although the above approach was thoroughly tested in a global NEMO simulation (Mathiot and Jourdain, 2023), participants are advised that this method can lead to potentially unphysical values for certain fields, such as negative shortwave radiation or relative humidities less than zero or above one hundred. We therefore advise participants to check their perturbed forcing fields and make corrections where needed.

2.3.5 Ice-sheet runoff

250 Besides ice-shelf melt fluxes, which are simulated in the models, additional sources of ice-sheet freshwater can alter the state of the ocean. These are iceberg calving, surface runoff from ice-sheet surface melting, and subglacial runoff, which can enhance the buoyancy of the water column near the ice-sheet grounding line. We do not impose any perturbations in these sources of solid or liquid runoff from the Antarctic Ice Sheet because they are not reliably represented in many models. Participants who use a Lagrangian iceberg model can keep the calving flux constant, so their total iceberg melt flux is 1100 Gt/yr for

255 both the present-day and the warm experiment, similar to (Mathiot and Jourdain, 2023). Due to warmer ocean conditions, the iceberg melt pattern may be shifted towards Antarctica in the future compared to present-day, while participants who impose an unperturbed freshwater flux at the surface will miss this effect. We nonetheless believe that this effect is small because 1) according to Mathiot and Jourdain (2023), ice-shelf melting in the warm experiment is more than 10 times larger than iceberg melting so that most additional freshwater will come from ice shelves, and 2) sea ice production is close to zero in

260 the warm experiment and the stratification therefore stops having a strong modulation role on deep convection. Regarding present-day and perturbed surface runoff and subglacial discharge, there is currently no consensus within the community about a preferred approach or dataset, and these sources are typically much smaller than the other ones previously mentioned. We therefore do not impose any stringent constraints on either flux.

2.3.6 Lateral Input/Forcing

265 In addition to the perturbation in atmospheric forcing, regional ocean configurations are requested to apply a prescribed perturbation to the lateral boundary conditions. Because of the abrupt change in atmospheric conditions, the proposed ocean simulations will be different from the actual IPSL-CM6A-LR ocean projections, as they won't represent slow warming of the deep ocean from 2015 to 2300. For this reason, the perturbation of the lateral boundary conditions for regional configurations is not taken from the IPSL-CM6A-LR projections, as this would make it difficult to compare global ocean models with no lateral

270 boundary conditions to regional domains. Taking zero perturbation at the lateral boundaries would raise a similar inconsistency between global and regional simulations, as (far-field) changes in the global ocean are not propagated into the regional domain. We therefore request that regional configurations apply ocean and sea ice anomalies at their boundaries taken from a global NEMO simulation (Mathiot and Jourdain, 2023) under the proposed atmospheric perturbation.

We provide the gridded average of the last 30 years of the present-day and perturbed state obtained by Mathiot and Jourdain

275 (2023). They are provided as the mean monthly values of ocean (temperature, salinity, velocities and sea surface height) and sea ice (fraction, ice and snow thickness, velocity) properties, and we let individual groups choose their method to calculate and prescribe the anomaly at the lateral boundaries as we consider it as part of the uncertainty. For example, Jourdain et al. (2022) prescribed anomalies in the geographical space while Naughten et al. (2023) prescribed anomalies in the temperature–salinity space. Although not mandatory, we encourage groups to apply anomalies in ocean velocities, e.g., through conservative

280 interpolation of the provided model outputs or by re-calculating geostrophic velocities from changes in temperature and salin-

ity (from vertically-integrated density gradients). Deriving the anomaly in barotropic velocity from the provided anomaly in barotropic stream function might also be useful for the various grids used in MISOMIP2.

Similar to the atmospheric perturbation, the present-day and perturbed ocean state of NEMO were calculated separately for each calendar month, i.e., they include a seasonal cycle. The corresponding anomalies should therefore be linearly interpolated
285 between the middle of two consecutive months to recreate a continuous perturbation.

We acknowledge that the NEMO anomaly cannot be considered as the true response, but this has been identified as the most consistent approach, and the variations across models will anyway be interpreted as a function of regional ocean warming in individual models.

2.4 OceanA-ctrl & OceanW-ctrl experiments

290 Because of possible model drifts in the absence of a perturbation, in particular for global models, we need a control simulation that is similar to the perturbed experiments(i.e. Ocean*-warm), but with zero anomaly in the forcing. All the sensitivity analyses will be undertaken with respect to this control simulation.

The OceanA-ctrl & OceanW-ctrl experiments represent extensions of the OceanA-hind & OceanW-hind experiments, obtained by cycling the forcing used in the latter. In the case where only one cycle of present-day conditions is used in OceanA-
295 warm and OceanW-warm experiments (i.e., $n = 0$ in Fig. 2 and Tab. 1), no extension is required. In other cases, the extension will start immediately after OceanA-hind & OceanW-hind, as shown in Fig. 2. Note that as for the OceanA-warm & OceanW-warm experiments, the time variable will continue forward for the time cycles, e.g., it will indicate 2015–2050 in an extension over a second cycle of the 1979–2014 present-day period.

2.5 OceanA-Pgeom, OceanA-Fgeom, OceanW-Pgeom & OceanW-Fgeom experiments

300 ### 2.5.1 Aim

These experiments will be used to compare the basal melt response to an imposed change in the geometry of the Amundsen and Weddell Seas ice-shelf cavities. Simulations are carried out with stand-alone ice-shelf–ocean models for two different ice-shelf cavity shapes: one present-day geometry (experiments Ocean*-Pgeom) and one hypothetical future geometry (experiments Ocean*-Fgeom). Further details about the geometries are provided below. The aim is to identify and compare the modelled
305 feedbacks between changes in cavity geometry, ocean circulation and basal melt rates for semi-realistic patterns of ice-shelf thinning and grounding line retreat. Such feedbacks have previously been shown to be important for the evolution of the ice-shelf mass balance over internanual to decadal timescales (e.g. Holland et al., 2023; De Rydt and Naughten, 2024).

2.5.2 Type of models

The model requirements are identical to those for the Ocean*-hind experiments. Models need to be able to implement the
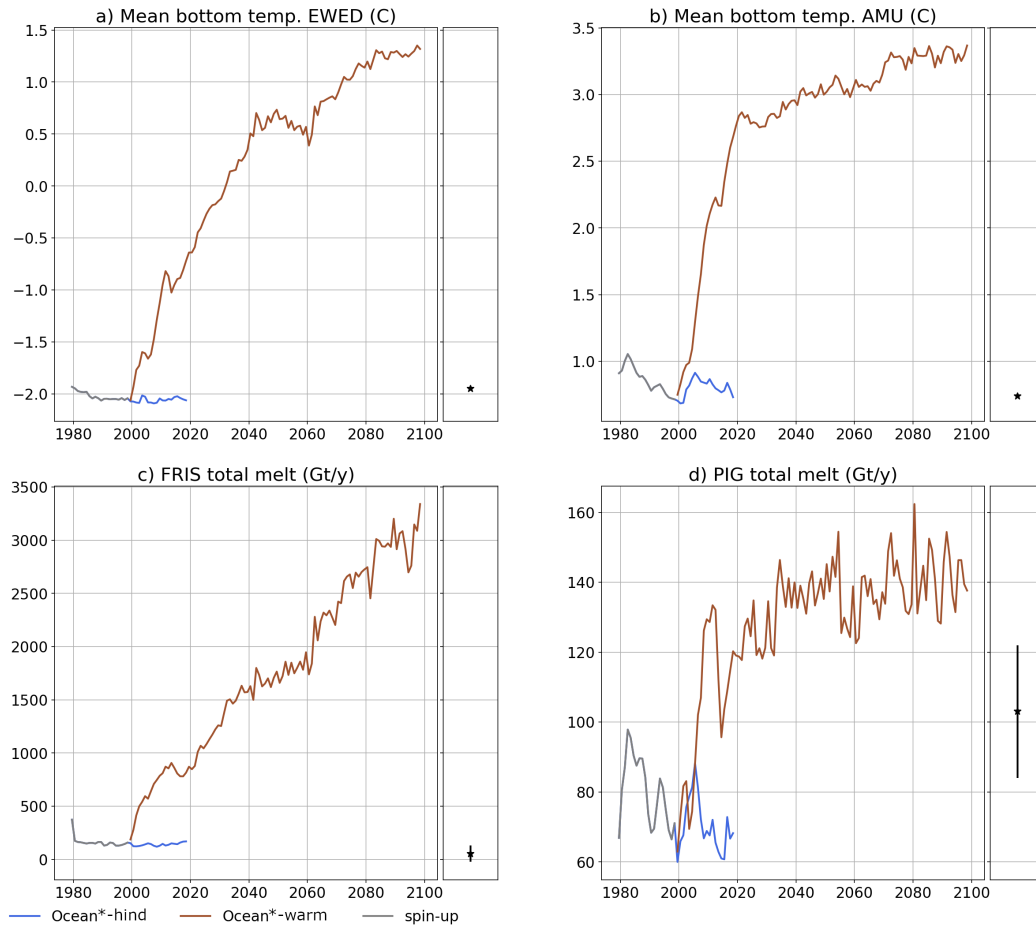310 prescribed ice-shelf geometries.

Figure 3. Example of results obtained by Mathiot and Jourdain (2023) in the OceanA-hind & OceanW-hind (blue) and OceanA-warm & OceanW-warm (brown) experiments. Top panels show the bottom temperature on the (a) East Weddell (EWED: 78.63-76.90°S; 45.65-32.25°W) and (b) Amundsen Sea (AMU: 75.80-71.66°S; 109.64-102.23°W) continental shelf. Lower panels show total melt integrated beneath (c) Filchner-Ronne and (d) Pine Island ice shelves (FRIS and PIG, respectively). Black stars on the right are the observational estimates from World Ocean Atlas 2018 (Locarnini et al., 2019) for the bottom temperature and from Paolo et al. (2023a) for the ice shelf melt. Here the perturbation experiment starts in 2000, and the anomaly is added to the 2000-2018 atmospheric forcing as well as to repeated cycles of the 1979-2018 forcing.

2.5.3 Time Window

Experiments with present-day and future cavity geometries both cover the same time window as Ocean*-hind, following a spin-up period with the imposed ice-shelf geometry, as shown in Figure 2. Present-day and future geometries each have their own spin-up.

2.5.4 Input/Forcing

The forcing is the same as for Ocean*-hind, i.e., the CAYA approach, except that a common bathymetry as well as present-day (OceanA-Pgeom & OceanW-Pgeom) and future (OceanA-Fgeom & OceanW-Fgeom) ice-shelf draft are imposed in the area from Dotson to Cosgrove (A) or in the region covered by the Filchner Ronne Ice Shelf (W).

For the Ocean*-Pgeom experiments, participants are asked to use the Bedmachine-Antarctica-v3 dataset (Morlighem, 2022) for the bathymetry and present-day ice draft. For some groups, this geometry might be very similar to the geometry in their Ocean*-hind experiments, for example when an earlier version of the Bedmachine dataset was used. For consistency, we ask participants to only provide results for the OceanA-Pgeom and OceanW-Pgeom experiments based on the exact Bedmachine-Antarctica-v3 topography.

For the OceanA-Fgeom and OceanW-Fgeom experiments, participants are asked to use the same bathymetry from Bedmachine-Antarctica-v3, but a modified ice-shelf draft. The latter is provided as part of the MIPkit, in the same format as Bedmachine-Antarctica-v3. The original Bedmachine-v3 values were left unchanged outside of the Amundsen and Weddell Seas regions, with a linear transition to the modified geometry over a 10 km halo. The future ice draft for the OceanA-Fgeom experiment was produced with the coupled ice-ocean model Úa-MITgcm, starting from a present-day ice-sheet geometry and forced by constant, shallow thermocline conditions on the Amundsen continental shelf for 200 years (De Rydt and Naughten, 2024) . The difference in ice thickness between the A-Pgeom and A-Fgeom geometries is shown in figure 4. For the OceanW-Fgeom experiment, the future ice draft is taken from an unpublished 300-year simulation with the coupled ice-ocean model Úa-MITgcm. The model configuration is identical to the abrupt-4xCO2 experiment described in (Naughten et al., 2021), but extended from 150 to 300 years based on a new timeseries of atmospheric and ocean boundary conditions from the UKESM-1-0-LL CMIP6 ensemble. The difference in ice thickness between the W-Pgeom and W-Fgeom geometry is shown in figure 4. Global or circum-Antarctic models can run the experiments in a single simulation.

2.6 IceOceanA-hind & IceOceanW-hind experiments

2.6.1 Aim

The objectives of the IceOceanA-hind and IceOceanW-hind experiments are analogous to MISOMIP1, but with a broader focus on model evaluation rather than verification of initial coupling developments. We invite contributions from coupled ice-sheet–ocean models to assess their ability to hindcast observed changes in ice volume, ice dynamics and grounding line location,
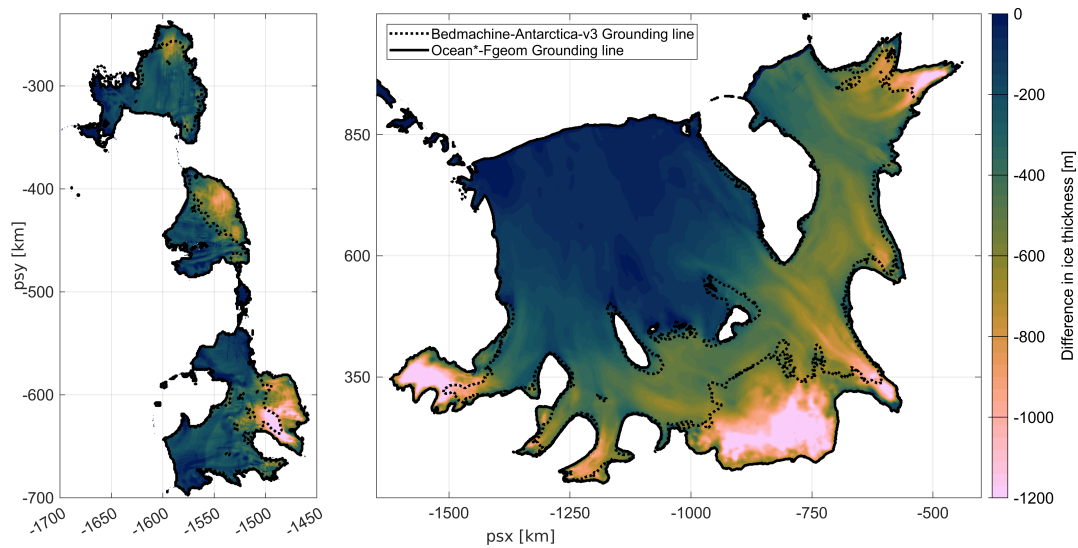
14

Figure 4. Difference in ice thickness between the Pgeom and Fgeom experiments for (a) the Amundsen Sea, and (b) the Weddell Sea. The geometry for the Pgeom experiments is taken from BedMachine Antarctica v3, the geometry for the Fgeom experiments is taken from Úa-MITgcm simulations, as described in the main text. The dotted and solid black lines correspond to the grounding lines for present-day (Pgeom) and future (Fgeom) geometries, respectively.

as well as ice-shelf melting and ocean changes. As with OceanA-hind & OceanW-hind, the MISOMIP2 protocol advocates a CAYA approach to these experiments.

The main focus of this exercise will be on the Amundsen Sea region, which has seen substantial changes over the 1990s-2020 time period, with a strong negative mass balance and a significant acceleration of mass loss. The Weddell Sea sector
345 has remained relatively unchanged and is assumed to be close to balance, but models need to be able to demonstrate this too, as capturing steady conditions can be challenging for some model set-ups (Comeau et al., 2022). Model outputs for these contrasting cases will be compared between different models, and to available oceanographic and glaciological observations.

2.6.2 Type of models

The experiments should be performed by coupled ice-sheet–ocean models, i.e., models in which the ocean state evolves as a
350 result of ice shelf melt and the evolution of ice shelf thickness and ice-sheet grounding lines. This includes the option of using coarse resolution ocean models coupled to an ice-sheet model through a parameterisation with no explicit representation of the ocean circulation in ice shelf cavities. Instead, a basal melt parameterization can be forced by 'far-field' ocean conditions, and the calculated meltwater added as a freshwater (virtual salt) flux at the front of the closed cavities (e.g., Kreuzer et al., 2021). There are no geographical restrictions on the ocean domain in these experiments. We also note that such ocean setups
355 should not contribute to the Ocean*-hind, Ocean*-Pgeom and Ocean*-Fgeom experiments, as they are targeting models with (thermo)dynamically interactive ice-shelf cavities.

15

The ocean model can be coupled to any type of ice-sheet/glacier model, from pan-Antarctic to smaller regional domains, ideally including the following drainage basins:

– For the Amundsen Sea: Pine Island, Thwaites, Smith, Pope, Kohler Glaciers.

– For the Weddell Sea: Evans, Carlson, Rutford, Institute, Moller, Foundation, Support Force, Recovery, Slessor and Bailey Ice Streams.

Additional levels of complexity in the coupling procedure involving, e.g., the evolution of the ice shelf calving front (Asay-Davis et al., 2016), the representation of iceberg drift (Smith et al., 2021), or subglacial freshwater discharge (Nakayama et al., 2021), are welcome but not required.

2.6.3 Time window

Models will ideally simulate ocean and ice dynamics over the past three decades (1990s-2020). If not possible, simulations should start in the mid 2000s at the latest. We welcome outputs starting earlier, e.g., from 1979, for models able to represent this period. However limited observations exists in the 1980s, so results from this time period will be use almost exclusively for model intercomparison.

2.6.4 Input/Forcing

Participants are encouraged to follow the CAYA approach, in particular with respect to the surface and lateral boundary conditions, with the loose constraint that the initial ice-sheet state should be as representative as possible of the geometry and dynamics observed a few decades ago. This can be obtained from a formal inversion using observations, from a calibrated or selected spin-up phase, or a combination of both. For example, for an initial configuration with nominal timestamp in the early 2000s, participants can use the Bedmachine bathymetry, the ICESat corrected ERS-1 DEM with a nominal timestamp of January 2004 (Bamber et al., 2009), and concurrent MeaSUREs surface velocity data (Mouginot et al., 2017b) to constrain their inversion. For an initial configuration in the mid to late 2000s, we recommend the use of recent topography products such as Bedmachine-Antarctica-v3 (Morlighem, 2022), and one of many suitable ice velocity products.

2.7 IceOceanA-warm & IceOceanW-warm experiments

These experiments undergo the same ocean perturbation and are run for the same duration as the OceanA-warm & OceanW-warm experiments. The ice-sheet surface mass balance and other potential surface conditions (e.g., atmospheric temperature above the ice sheet) remain unchanged compared to IceOceanA-hind & IceOceanW-hind. The requested outputs are the same as IceOceanA-hind & IceOceanW-hind with a continuous time variable over several cycles of the present-day period.

2.8 IceOceanA-ctrl & IceOceanW-ctrl experiments

This is an extension of IceOceanA-hind & IceOceanW-hind over several present-day cycles, and therefore with repeated conditions similar to present, to be used as control for the IceOceanA-warm and IceOceanW-warm experiments.

3 MIPkit

For both the Amundsen and Weddell sectors, the initial version of the MIPkit consists of ocean and ice data that are formatted to be directly comparable to the model outputs (described in the next section), as well as the input files needed for coordinated perturbation experiments. In summary:

– Instantaneous ocean temperature (T) and salinity (S) sampled on horizontal depth levels at 100, 200, 300, 400, 500, 600, 700, 800, 900, 1000, and 1500 meter, from available CTDs in the intercomparison domain. These observations will be used for the evaluation of large-scale hydrographic structures.

– Instantaneous ocean T,S from CTDs on a few chosen vertical sections at higher vertical resolution, which will be used for finer evaluation of the thermocline and pycnocline evolution across the continental shelf.

– Monthly-mean T,S at a few mooring sites providing a longer observational window (seasonal and interannual).

– Annual ice surface velocities and surface elevation changes from available earth observation products will be used for the evaluation of the present-day state of the ice sheet and its dynamical evolution over the observational period. We do not expect participants to use these data to initialize their models, but they can be a helpful tool to evaluate their setups.

– Perturbed atmospheric forcing ("warm" experiments) and ice-sheet perturbed geometry (A-Fgeom/W-Fgeom experiments).

Importantly, the provided CTD measurements are representative of summer conditions, so model outputs will need to be considered in summer as well for evaluation.

We may evaluate the simulated ice-shelf basal melt rates based on several types of data, including autonomous phase-sensitive radio-echo sounder (ApRES), which will be facilitated by the NECKLACE project (https://necklaceproject.com), estimates from remote sensing and regional climate models (Rignot et al., 2013; Moholdt et al., 2014; Shean et al., 2019; Adusumilli et al., 2020; Paolo et al., 2023a), and estimates from CTD measurements (?Dutrieux et al., 2014; Jenkins et al., 2018). However, ApRES tend to resolve finer spatial scales than those resolved in models, and other methods have large and somewhat unconstrained error bars over short to interannual time scales, so the use of these data in MISOMIP2 will be discussed during the result analysis.

The different parts of the MIPkit are gathered in the MISOMIP2 community on Zenodo: https://zenodo.org/communities/misomip2.

3.1 MIPkit–A (Amundsen)

MIPkit–A contains both ice-sheet and ocean data. For the ice-sheet, annual maps of ice surface velocity and surface elevation change are provided for the time periods 2000-2019 and 1992-2019 respectively. The datasets were compiled from available Earth observation data, and linearly interpolated onto the MISOMIP2 common grid (Table 4). For the surface velocities, a weighted average of data from the MeaSUREs project (Rignot et al., 2014b; Mouginot et al., 2017a) and MeaSUREs ITS_LIVE project (Gardner et al., 2022) is provided, with weights corresponding to the inverse square error of the original datasets. For the surface elevation changes, a weighted average of data from CPOM data (Otosaka et al., 2023; Bevan et al., 2023) and MeaSUREs ITS_LIVE data (Nilsson et al., 2023) for the grounded ice and MeaSUREs ITS_LIVE data (Paolo et al., 2023a, b) for floating ice is provided. Both data sets include propagated errors and a mask indicating the original data sources for each grid point.

The ocean data consists of hydrographic properties along horizontal and vertical sections. The hydrographic properties provided on horizontal sections at 15 depths (every 100 m) come from the CTD measurements obtained during cruises of the following icebreaker research vessels Nathaniel B. Palmer (United States Antarctic Program) , James Clark Ross (British Antarctic Survey and Natural Environment Research Council), Araon (Korea Polar Research Institute), Oden (Swedish Polar Research), and Polarstern (Alfred Wegener Institute, Germany). Here we have gathered data for the first months of 1994 (Jacobs, 1994), 2000 (Jacobs, 2000), 2007 (Jacobs, 2007), 2009 (Jacobs, 2009), 2010 (Swedish Polar Research Secretariat, 2010; Gohl, 2015), 2012 (Kim et al., 2012), 2014 (Heywood, 2014; **?**), 2016 (Kim et al., 2016), 2017 (Gohl, 2017), 2018 (Kim et al., 2018), 2019 (Larter et al., 2019) and 2020 (Wellner, 2020).

These data have been used in a number of scientific studies, from the discovery of intrusions of warm deep water towards peripheral Antarctic ice shelves (**?**) to the description of the interannual variability of ocean properties on the continental shelf (e.g., **?**Nakayama et al., 2013; Dutrieux et al., 2014; Heywood et al., 2016; Kim et al., 2016; Webber et al., 2017; Jenkins et al., 2018). In front of the Pine Island and Dotson ice shelves, the thermocline rose in the mid 2000s and remained high from 2006 to 2011, associated with an increased heat content over the continental shelf. The thermocline was back to a relatively deep position from 2012 to 2017 (Naughten et al., 2022).

The first vertical section where we provide hydrographic data in the Amundsen Sea starts across the continental shelf break and follows the Eastern Pine Island Trough southward until Pine Island Ice Shelf. This section was monitored by the following cruises: N.B. Palmer in January 2009, Polarstern in March 2010 and Araon in February-March 2012 (**?**Gohl, 2015; Dutrieux et al., 2014). The second vertical section starts across the continental shelf break and follows the Dotson-Getz Trough southward until the Dotson Ice Shelf. It was monitored by the aforementioned Araon expeditions in 2010–2011 and early 2012 (Kim et al., 2017).

We will also conduct model-data comparisons for multi-year mooring observations (Tab. 3). The first mooring site is located near the northern part of the Pine Island ice shelf front (102.07°W, 74.87°S) and captures the thermocline variability from 2012 to 2018 ("iSTAR-8" in the NERC iSTAR program, and "pig-n" in the NERC Ocean Forcing Ice Change Program). The second mooring site is located near the southern part of the Pine Island ice shelf front (102.15°W, 75.05°S), was monitored

between 2009 and 2016, then in 2019–2020 through the following moorings: "BSR-5" (Buoy Supported Riser, Jacobs, 2009), "iSTAR-9" (NERC iSTAR Program), and "pig-s" (NERC Ocean Forcing Ice Change Program). This second site experienced a strong deepening of the thermocline in 2012–2013 (Webber et al., 2017), then a more moderate deepening in 2016. These two mooring sites are located only 20 km from each other, show distinct mean thermocline depth and more consistent variability (Joughin et al., 2021).

The third mooring observation ("trough-e" in the NERC Ocean Forcing Ice Change Program) used in MISOMIP2 is at the eastern Pine Island trough (102.55°W, 71.33°S). The eastern trough is considered to be the entrance of modified Circumpolar Deep Water reaching the Pine Island Ice Shelf (?Nakayama et al., 2013; Webber et al., 2017) but only two years of mooring observation was conducted from 2014-2015 due to sea ice cover.

The fourth mooring site used in MISOMIP2 is at the western Pine Island trough (113.05°W, 71.56°S). Several mooring observations were conducted within 2 km of each other, allowing us to observe thermocline variability from 2009 to 2016 with one year gap in 2011: "BSR-12" (Jacobs, 2009), "iSTAR-1" (NERC iSTAR Program), and "trough-w" (NERC Ocean Forcing Ice Change Program).

The fifth mooring observation ("mid-shelf" in the NERC Ocean Forcing Ice Change Program) used in MISOMIP2 is at the middle of the eastern Amunsen Sea in the submarine glacial trough connecting open water and Pine Island and Thwaites ice shelves (106.53°W, 73.81°S). Two mooring observations were conducted within a few kilometers of each other, allowing us to observe thermocline variability from 2012 to 2018: "iSTAR-6" (NERC iSTAR Program), and "mid-shelf" (NERC Ocean Forcing Ice Change Program).

The sixth and seventh moorings used in MISOMIP2 are located in the Getz-Dotson trough (114.99°W, 71.16°S and 118.46°W, 71.96°S). They were originally deployed under the names "BSR-7" and "BSR-14" (Jacobs, 2009) and further deployments were conducted by the Korea Polar Research Institute. These mooring observations have been used to study the inflow of warm ocean heat towards the Getz and Dotson ice shelves (Kim et al., 2016, 2017, 2018).

The eighth mooring used in MISOMIP2 is located beneath the Thwaites ice shelf (104.83°W, 75.21°S) and has been used to study ice shelf cavity environment in 2020–2021 (Davis et al., 2021, 2023).

3.2 MIPkit–W (Weddell)

Similar to MIPkit–A, the MIPkit–W contains both ice-sheet and ocean data. The ice-sheet data was obtained from the same data sources and using the same methods as described in section 3.1 for MIPkit–A.

For the evaluation of the ocean model performance in the Weddell Sea sector we focus on the interaction between the far-field general circulation and the processes on the continental shelf and in the ice-shelf cavities.

The hydrographic properties provided on horizontal sections at 15 depths have been derived from the CTD measurements obtained from late December to early March by the Alfred Wegener Institute, Bremerhaven (AWI) during Polarstern cruises ANT-XII/3 (Schröder, 2010), PS82 (Schröder and Wisotzki, 2014), PS96 (Schröder et al., 2016) and PS111 (Janout et al., 2019), which cover years 1995, 2014, 2016 and 2018, respectively.

The first vertical section where we provide hydrographic data goes from the tip of the Antarctic Peninsula to Kapp Norwegia (12.33°E). It is known as WOCE-SR04 and has been monitored since 1989. It captures both the water masses that feed the continental shelf and those that have been modified by ice shelf–ocean interaction, including newly formed bottom water. The surface water and the subsurface Winter Water influence the sea-ice formation and thus the production of the High Salinity Shelf Water (HSSW) that enters FRIS cavity. The intermediate Warm Deep Water (WDW), i.e., the Circumpolar Deep Water upwelled in the Weddell Sea, is an important heat source that —modified to some degree— episodically enters the Filchner Through and might reach the cavity (Ryan et al., 2020). The water masses below WDW, i.e., the Weddell Sea Deep Water (WSDW) and Weddell Sea Bottom Water (WSBW) are products of mixing between the HSSW and the Ice Shelf Water (ISW) formed in the depths of the FRIS cavity. The data provided were collected during Polarstern cruises in Sep.-Oct. 1989, Nov.-Dec. 1990, Dec. 1992-Jan. 1993, Mar.-May 1996, Apr.-May 1998 (Fahrbach and Rohardt, 1990, 1991, 1993, 1996, 1998), Jan.-Apr. 2005 (Rohardt, 2010), Feb.-Apr. 2008 (Fahrbach and Rohardt, 2008), Dec. 2010-Jan. 2011 (Rohardt et al., 2011), Dec. 2012-Jan. 2013 (Rohardt, 2013), as well as Dec. 2016-Jan. 2017 and Dec. 2018-Feb. 2019 (Rohardt and Boebel, 2017, 2020).

The second vertical section is at ∼76°S and covers the eastern side of Filchner Through. It was surveyed during some of the aforementioned Polarstern cruises on 5-8 Jan. 2014, 20-24 Jan. 2016 and 4-23 Feb. 2018. These sections show episodic signs of intruding modified WDW.

The third and fourth sections were obtained along the front of Ronne and Filchner ice shelves, respectively. The Filchner section was measured on 1-3 Feb. 1977 (Foldvik et al., 1985) and 7-16 Jan. 1981 (Hubold et al., 1982) from the Norwegian Research Vessel "Polarsirkel", then during several of the Polarstern cruises: 25 Jan.- 4 Mar. 1995, 15-17 Jan. 2014, 15 Jan. 2016 (only one vertical profile), and 14-23 Feb. 2018. The Ronne section was measured on 25 Jan.- 24 Feb. 1995, 14-15 Jan. 2016, and 9-14 Feb. 2018 in the continuity of the Filchner section. These sections showed the properties and location of in- and outflow to/from the ice shelf cavity and their variability.

Finally, three moorings placed along the 76°S vertical section give an insight into the variability of intrusions of modified WDW and five moorings underneath Filchner-Ronne Ice Shelf to access the intrusion of HSSW and production of ISW. The 76°S moorings are originally referred to as AWI252 (30.47°W), AWI253 (30.99°W) and AWI254 (31.48°W), and cover the period from Jan. 2014 to Feb. 2018 (Schröder et al., 2017a, b, c, 2019a, b, c). Temperature, salinity and velocity data were obtained at two depths for AWI252 (335 and 421 m depth for a seafloor at 447 m) and AWI253 (349 and 434 m depth for a seafloor at 456 m), while a single depth is provided for AWI254 (553 m for a seafloor at 581 m). The moorings under the ice shelf were designed to collect data representative of the entire water column from the ice shelf base to the seafloor at each location and capture interannual variability linked to large-scale atmospheric circulation (Hattermann et al., 2021). For our goals we provide monthly means but it is important to mention that the area is influenced by high frequency variability.

3.3 MIPkit–Perturbations

This MIPkit contains all data needed to run the perturbation experiments: the perturbations to add to the atmospheric forcing and possibly to the ocean lateral boundaries (A-warm and W-warm experiments), as well as the perturbed ice-shelf geometry (A-Fgeom, W-Fgeom). More details are provided in section 2.

3.4 Living MIPkit

While an effort has been made to gather existing Earth observation and in situ data for the ice sheet and ocean as part of the initial release of the MISOMIP2 protocol, we consider the MIPkit to be a living archive. We expect the MIPkit to be updated with new observational products reformatted for MISOMIP2 as necessary. The on-going updates will be associated with version numbers on Zenodo. The MIPkit is nonetheless not intended to be a complete archive of all available data, rather a representative subset of observations that have been reformatted for easy comparison to the required model output.

4 Requested model outputs

Although we do not plan to upload the MISOMIP2 data onto the Earth System Grid Federation (ESGF) to keep some flexibility, we believe that a step toward more standardisation than in MISOMIP1 will make our intercomparison more robust and reproducible, and will facilitate potential future contributions of our community to CMIP and ISMIP.

For all the outputs described hereafter, we encourage participants to use the NetCDF-4 format with a simple precision for floats, a deflation level of 1 and chunking along the vertical and time dimensions set to 1, which should save space and facilitate the data processing.

4.1 Ocean outputs

Monthly mean outputs will be submitted on standard horizontal and vertical grids: a three-dimensional grid with few vertical levels used to plot horizontal slices, a few vertical sections to coincide with ship borne CTD sections (included in the MIPkit), and a few profiles at a single location for direct comparison to existing mooring data (included in the MIPkit). An overview of the sections and mooring profiles in the MIPkit, as well as the requested locations for model sections and profiles is provide in Fig. 1. The common grids, list of requested variables and recommended interpolation methods are provided below.

4.1.1 File naming convention and common grids

Three types of files will be provided by participants:

- `Oce3d_<institute>_<model>_<abc>_<exp>_<period>.nc`

- `OceSec<n>_<institute>_<model>_<abc>_<exp>_<period>.nc`

- `OceMoor<n>_<institute>_<model>_<abc>_<exp>_<period>.nc`

21

where `<n>` is the section or mooring number, `<model>` is the model name, possibly including a version number, `<institute>` is the name of the institute(s) that produced the simulation (use "−" rather than "_" for multiple entities), `<abc>` is a single letter used to distinguish multiple set-ups produced by a given institute (e.g., variation of model parameters, resolution, initial states or boundary conditions), `<exp>` is the MISOMIP2 experiment name (e.g., `OceanA-hind`, `OceanW-hind`, `IceOceanA-hind`, ...), and `<period>` indicates the starting year and month and the final year and month (e.g., 197901-202012). The simulations can be split into as many time segments as desired. Note that modelling groups that provide regional simulations for both the Amundsen and Weddell sectors should use the same letter in `<abc>` only if the modelling set-up is exactly the same (apart from the domain location).

- The `Oce3d` files cover monthly mean fields on the three-dimensional common grids described in Tab. 2 and shown in Fig. 1, and contain all the ocean variables discussed hereafter.

- The `OceSec` files contain potential temperature and salinity along six observed vertical sections, four in the Weddell Sea and two in the Amundsen Sea, as described in Sect. 3. The (`lon`,`lat`,`lev`) locations of the requested data are provided in `preproc/def_grids.py` on https://github.com/misomip/misomip2 or as `.csv` files in the MIPkit–A and MIPkit–W datasets (https://zenodo.org/communities/misomip2). Vertical coordinates are uniformly spaced at 10 m intervals between 0 m and 1150 m, except for the SR04 section between Kapp Norvegia and the tip of the Antarctic Peninsula, for which data should be provided at 10 m depth intervals between 0 m and 5000 m.

- The `OceMoor` files contain vertical profiles of potential temperature and salinity at 16 locations, listed in Tab. 3. At each location, the data is requested at 1 m vertical resolution between 0 m and 1150 m. The (`lon`,`lat`,`lev`) coordinates in Tab. 3 are also available in `preproc/def_grids.py` on https://github.com/misomip/misomip2 or as `.csv` files in the MIPkit–A and MIPkit–W datasets.

Table 2. Common grid parameters used for Oce3d files.

	longitude	latitude	resolution (lon×lat)	depth (m)
Amundsen Sea	140°W–90°W	76°S–69°S	1/10° × 1/30°	0,100,...,900,1000,1500
Weddell Sea	90°W– 0°E	85°S–60°S	1/3° × 1/10°	0,100,...,900,1000,1500

4.1.2 Dimensions, variables and metadata

The requested output format follows the NetCDF Climate and Forecast (CF) Metadata Conventions. The dimensions of the common ocean grids are (`lon`,`lat`,`lev`,`time`,`bnds`), and their corresponding variables and attributes are defined in Appendix (Tab. A1).

The requested ocean variables are listed in Tabs. A1-A5. They are largely based on the CMIP6 data request and on the OMIP variables described in the appendices of Griffies et al. (2016), with additional variables introduced here to describe

Table 3. Location of mooring data.

sector	mooring	longitude	latitude	vertical discretisation (m)
Amundsen	Moor1	102.08°W	74.87°S	0, 1, 2, ..., 1150
	Moor2	102.15°W	75.06°S	0, 1, 2, ..., 1150
	Moor3	102.55°W	71.33°S	0, 1, 2, ..., 1150
	Moor5	106.53°W	73.81°S	0, 1, 2, ..., 1150
	Moor6	114.98°W	73.16°S	0, 1, 2, ..., 1150
	Moor7	118.46°W	71.96°S	0, 1, 2, ..., 1150
	Moor8	104.83°W	75.21°S	0, 1, 2, ..., 1150
Weddell	Moor1	30.47°W	76.09°S	0, 1, 2, ..., 1150
	Moor2	30.99°W	76.05°S	0, 1, 2, ..., 1150
	Moor3	31.48°W	75.96°S	0, 1, 2, ..., 1150
	Moor4	54.71°W	80.29°S	0, 1, 2, ..., 1150
	Moor5	44.43°W	80.44°S	0, 1, 2, ..., 1150
	Moor6	40.83°W	81.08°S	0, 1, 2, ..., 1150
	Moor7	37.26°W	78.54°S	0, 1, 2, ..., 1150
	Moor8	38.09°W	78.56°S	0, 1, 2, ..., 1150

565 ice-shelf cavities and ice-shelf–ocean interactions, as well as a few new variables that are the sum of existing variables (underlined variables in Tabs. A1-A5). Note that for the perturbation experiments (Ocean*-warm, Ocean*-ctrl, IceOcean*-warm and IceOcean*-ctrl) the time variable will continue forward over the time cycles, e.g., it will indicate 2001–2040 for two consecutive cycles forced by 2001–2020 boundary conditions.

Although several models have transitioned to the TEOS10 seawater thermodynamics which is formulated for a better repre-
570 sentation of heat conservation and of the chemical compositions of seawater (IOC et al., 2010), many model formulations are still based on pre-TEOS10 thermodynamics. For simplicity, we make the choice to stick to this formulation for MISOMIP2, although we believe that future intercomparisons would benefit from transitioning towards TEOS10. Models that archived TEOS10 quantities may use the Gibbs Sea Water oceanographic toolbox to convert to pre-TEOS10 quantities.

All time-dependent ocean variables are monthly means (over full calendar months). All these variables have a fill value
575 (_FillValue) set to 9.969209968386869e36 (standard missing value for floats in NetCDF); this value is attributed to any part of the MISOMIP2 domain that is not covered by the original domain (no extrapolation), and to cell fractions lower than 1% (e.g., all the variables interpolated from ice-shelf cells are set to the fill value if the interpolated ice-shelf fraction is lower than 1%). Note that according to this framework, some cells with a partial ice-shelf fraction have both a non-zero ice-shelf draft and non-zero sea surface fraction with corresponding surface temperature, salinity, etc.

580 We recommend that participants add a `warning` attribute for any variable that was recalculated offline based on specific assumptions, interpolated in an atypical way, or where its interpretation might otherwise require caveats.

We ask all contributors to indicate the main aspects of their modelling set-up as global attributes in the NetCDF files. This is an important part of the output that will facilitate automatic display, analysis and clustering of multi-model outputs. The requested global attributes for ocean outputs are listed in Tabs. A7-A8.

4.1.3 Interpolation methods

Because of the imposed regridding to the common grid, it is essential to clarify the interpolation method.

Conservative interpolation of coarse resolution model output onto a fine grid imprints the coarse grid meshes (e.g. big rectangles) on the fine grid. When averaging multiple models, this may hide dynamical structures such as gyres and horizontal gradients. We therefore do not recommend using conservative interpolation for model grids of similar or coarser resolution than the MISOMIP2 standard grids. Instead, we recommend linear interpolation in the $(\text{lon} \times \cos\langle\text{lat}\rangle, \text{lat})$ space for all variables, where $\langle\text{lat}\rangle$ is the mean latitude over the MISOMIP domain. This is preferred to an interpolation in the (lon,lat) space to have a more isotropic interpolation. As there are a variety of grid structures and projections, we recommend the linear triangular interpolation which may be suitable for all models. It consists of triangulating the input data and performing a linear interpolation in the barycentric coordinate system. For target points falling out of the convex zone, no triangular interpolation is possible, and a nearest-neighbor interpolation is recommended to fill these points. Bi-linear interpolation can also be performed for models on structured lon-lat grids, and other similar linear methods are also accepted (e.g., `ESMF_RegridWeightGen` from the ESMF library). For model grids of significantly higher resolution than the standard MISOMIP2 grid, conservative interpolation or average-based grid coarsening prior to linear interpolation are reasonable options.

For the model intercomparison, it is essential that interpolations consider whether a given variable is defined over the entire cell or only over a fraction of it. This is indicated through the `cell_methods` attribute in Tabs.A1-A5:

- `area: mean` indicates interpolation from all neighbour cells.

- `area: mean where sea ice` indicates interpolation from neighbour cells weighted by their sea-ice fraction.

- `area: mean where ice shelf` indicates interpolation from neighbour cells weighted by their ice-shelf fraction.

- `area: mean over bottom ocean cells` indicates interpolation from neighbour bottom ocean cells.

- `area: mean where ocean surface` indicates interpolation from neighbour cells with ocean or sea-ice at the surface (ice shelves excluded).

- `area: mean where 3d ocean` indicates interpolation from neighbour cells with ocean at any depth (i.e., including ice-shelf cavities).

- `volume: mean where ocean` indicates 3D interpolation from neighbour ocean cells.

The recommended vertical interpolation method is a simple one-dimensional linear interpolation in depth coordinates. Non-Z-coordinate models therefore need to convert their outputs to Z coordinates prior to interpolation to the MISOMIP2 grids.

Several vertical coordinate systems may depend on sea surface height, which makes vertical levels fluctuate by a few meters at most. In MISOMIP2, we tolerate that this is not accounted for in the vertical interpolation as it can greatly facilitate computations without altering the intercomparison to a significant extent. The interpolated value should cover the entire model wet cells, and uniform values can be used beyond the centre of the uppermost and lowermost cells.

4.2 Ice Outputs

In addition to the aforementioned ocean outputs, all participants will provide yearly snapshots or means for a range of ice-sheet variables, including ice thickness, ice velocities, and grounding line location, on a predefined horizontal grid. The common grids, list of requested variables (largely based on ISMIP6 requested variables, see Nowicki et al., 2016) and recommended interpolation methods are listed here.

File naming convention and common grids:

In MISOMIP2, we only request 2D ice-sheet variables, provided as snapshots or yearly averages at the end of each year. Variables should be vertically averaged and interpolated onto cell centers of a regular horizontal grid with uniform horizontal resolution of 1 kilometer. The characteristics of the common grids for the Amundsen Sea and Weddell Sea domains are provided in Tab. 4 and shown in Fig. 1.

Table 4. Boundaries, resolution and number of points of the standard ice grids. Coordinates use the EPSG:3031 Antarctic Polar Stereographic projection with standard parallel -71°S and central meridian 0°W.

	x [m]	y [m]	resolution [m]	nx	ny
Amundsen	[-1847000 : -997000]	[-860000 : 104000]	1000 × 1000	850	964
Weddell	[-1683000 : 923000]	[-195000 : 1648000]	1000 × 1000	2606	1843

Only one type of file will be provided by participants for ice outputs:

– `Ice_<model>_<institute>_<abc>_<exp>_<period>.nc`

where `<model>`, `<institute>`, `<abc>`, `<exp>` and `<period>` are defined in the previous subsection.

Dimensions, variables and metadata:

The requested output format follows the NetCDF Climate and Forecast (CF) Metadata Conventions. The dimensions of the common ice-sheet grids are (`x`,`y`,`time`,`bnds`), and their corresponding variables and attributes are defined in Tab. A9.

The requested ice variables are listed in Tabs. A9-A12. They are largely based on the CMIP6 data request and on the ISMIP6 variables described in Nowicki et al. (2016).

Interpolation methods:

In contrast to ISMIP6, the primary aim of MISOMIP2 is to analyse dynamical patterns across a large range of model resolutions, rather than to accurately quantify the evolution of the ice-sheet mass. Therefore, we do not request conservative interpolation. In the case of participating ice-sheet model grids that are much coarser than the 1-km common grid, linear

interpolation methods (see examples in the previous subsection) should be preferred to conservative and nearest-neighbour interpolations, to avoid misleading strong gradients on the common grid.

640   For the intercomparison between models, it is essential that interpolations consider whether a given variable is defined over the entire cell or only over a fraction of the cell. This is indicated through the `cell_methods` attribute in Tabs. A9-A12:

- `area: mean` indicates interpolation from all neighbouring cells, including nunataks, ocean, ice sheet.

- `area: mean where land ice` indicates interpolation from neighbouring cells weighted by their land-ice fraction (grounded or floating).

645   - `area: mean where ice shelf` indicates interpolation from neighbouring cells weighted by their ice-shelf fraction.

- `area: mean where grounded ice` indicates interpolation from neighbouring cells weighted by their grounded ice fraction.

As in ISMIP6, we require snapshots for the state variables and yearly averages for the flux and tendency variables. This
650   is indicated in in Tabs. A9-A12 through the `cell_methods` attribute, which contains either `time: instantaneous` or `time: yearly mean`.

We ask all contributors to indicate the main aspects of their modelling set-up as global attributes in the NetCDF files in a way to facilitate automatic display, analysis and clustering of multi-model outputs. The global attributes of the ice output file are listed in Tab. A13.

655   ## 5   Conclusions and outlook

We have described the design of several interrelated ocean and coupled ice-sheet–ocean experiments for two targeted regions of Antarctica, collectively referred to as the Marine Ice Sheet Ocean Model Intercomparison Project - phase 2 (MISOMIP2). A series of ocean-only and coupled ice-sheet–ocean experiments were designed to test model fidelity and model sensitivity to a large, prescribed anomaly in climate forcing. We expect that results from each part (ocean-only and coupled ocean–ice) will be
660   published separately with all contributors as coauthors, following the tradition of earlier MIPs. We have tested the feasibility of all standalone ocean and ice-sheet–ocean experiments using several ocean and ice-sheet–ocean configurations, and we are confident that they can be run by other participants who use different model architectures and climatic forcing datasets. Future community activities will be determined based on the outcomes of the MISOMIP2 experiments. These potentially include, but are not limited to, experiments with a higher degree of similarity in climate forcing between contributing models, parameter and
665   numerical choices, and forward simulations at multi-decadal to century timescales under a range of prescribed climate-change scenarios, aimed at coordinating with ongoing ISMIP and CMIP efforts.

Code and data availability. All the code and data provided for the MISOMIP2 experiments, from pre-processing to post-processing, are and will be shared within the MISOMIP2 Zenodo community (https://zenodo.org/communities/misomip2) and on GitHub (https://github.com/misomip/misomip2). As ice-sheet modellers previously developed scripts to interpolate their outputs onto the ISMIP6 stereographic grid, we have not developed any processing tool for ice sheet models. The shared data include:

670

- MIPkit–A (Amundsen observational data): https://zenodo.org/doi/10.5281/zenodo.10062355

- MIPkit–W (Weddell observational data): https://zenodo.org/doi/10.5281/zenodo.8316180

- MIPkit–Perturbation: https://zenodo.org/doi/10.5281/zenodo.10046053

- Python tools that can be used to prepare the ocean data (https://github.com/misomip/misomip2), including:

675

  - the ocean grids definition in `preproc/def_grids.py`;

  - the definition of attributes for individual variables in `preproc/def_attrs.py`;

  - an example of inclusion of global attributes in `examples/interpolate_to_common_grid_oce.py`.

  - full interpolation procedure, currently only implemented for examples from NEMO, MITgcm and ROMS which are provided on https://doi.org/10.5281/zenodo.4709850 although this could be generalised to other models, including with unstructured grids.

680

- Analysis tools will be shared progressively on https://github.com/misomip/misomip2.

27

Table A1. Requested ocean variables and their attributes. Variables that are modified or newly introduced in this article are underlined. For time dependent variables, monthly mean outputs are requested.

variable (dimensions)	attribute name	attribute value
lon (lon)	long_name	"Longitude"
	units	"degrees_east"
	standard_name	"longitude"
	comment	common MISOMIP2 grid
lat (lat)	long_name	"Latitude"
	units	"degrees_north"
	standard_name	"latitude"
	comment	common MISOMIP2 grid
lev (lev)	long_name	"depth"
	units	"m"
	positive	"down"
	comment	common MISOMIP2 grid; increases from the sea surface to the sea floor
time (time)	long_name	"time"
	units	"days since 1900-1-1 0:0:0" or "seconds since 1900-1-1 0:0:0", or since any other date.
	standard_name	"time"
	calendar	"standard" (same as "gregorian" for recent centuries) for actual dates, or any other calendar, e.g. "no_leap" or "360_day"
	bounds	"time_bounds"
	comment	the time_bounds variable should be defined with dimensions (time,bnds) to indicate the beginning and end of the months over which the monthly averages are done
sftflf ([time,]lat,lon)	long_name	"Floating Ice Shelf Area Percentage"
	units	"%"
	standard_name	"floating_ice_shelf_area_fraction"
	cell_methods	"area: mean[; time: monthly mean]"
	comment	Time-dependent for coupled ocean–ice simulations or prescribed changes
sftof ([time,]lat,lon)	long_name	"Sea Area Percentage at the Surface"
	units	"%"
	standard_name	sea_area_fraction
	cell_methods	"area: mean[; time: monthly mean]"
	comment	Equals zero if sftflf is 100% (ice shelf) or if the cell is fully occupied by land, but 100% for a cell fully or partially covered with sea ice; time-dependent for coupled ocean–ice simulations or prescribed changes.
levof ([time,]lev,lat,lon)	long_name	"Sea area fraction at each vertical level"
	units	"%"
	standard_name	
	cell_methods	"area: mean[; time: monthly mean]"
	comment	Time-dependent for coupled ocean–ice simulations or prescribed changes.

Table A2. Continuation of Tab. A1

deptho	long_name	"Sea Floor Depth Below Geoid"
([time,]lat,lon)	units	"m"
	standard_name	"sea_floor_depth_below_geoid"
	cell_methods	"area: mean where 3d ocean[; time: monthly mean]"
	comment	Possibly time-dependent if glacial isostasy or bathymetry corrections are implemented.
depflf	long_name	"Depth of Floating Ice Shelf Base Below Geoid"
([time,]lat,lon)	units	"m"
	standard_name	
	cell_methods	"area: mean where ice shelf[; time: monthly mean]"
	comment	Time-dependent for coupled ocean–ice simulations or prescribed changes.
thetao	long_name	"Sea Water Potential Temperature"
(time,lev,lat,lon)	units	"degC"
	standard_name	"sea_water_potential_temperature"
	cell_methods	"volume: mean where ocean; time: monthly mean"
so	long_name	"Sea Water Salinity"
(time,lev,lat,lon)	units	"0.001"
	standard_name	"sea_water_salinity"
	cell_methods	"volume: mean where ocean; time: monthly mean"
	comment	This is the quantity that approximates the practical salinity traditionally obtained through conductivity measurements (see appendix D of Griffies et al., 2016).
tob	long_name	"Sea Water Potential Temperature at Sea Floor"
(time,lat,lon)	units	"degC"
	standard_name	"sea_water_potential_temperature_at_sea_floor"
	cell_methods	"area: mean where bottom ocean; time: monthly mean"
sob	long_name	"Sea Water Salinity at Sea Floor"
(time,lat,lon)	units	"0.001"
	standard_name	"sea_water_salinity_at_sea_floor"
	cell_methods	"area: mean where bottom ocean; time: monthly mean"
	comment	This is practical salinity.

Table A3. Continuation of Tab. A1

uo	long_name	"Sea Water X Velocity"
(time,lev,lat,lon)	units	"m s-1"
	standard_name	"sea_water_x_velocity"
	cell_methods	"volume: mean where ocean; time: monthly mean"
	comment	This is zonal velocity on the common grid, positive eastward
vo	long_name	"Sea Water Y Velocity"
(time,lev,lat,lon)	units	"m s-1"
	standard_name	"sea_water_y_velocity"
	cell_methods	"volume: mean where ocean; time: monthly mean"
	comment	This is meridional velocity on the common grid, positive northward
tauuo	long_name	"Sea Water Downward X Stress"
(time,lat,lon)	units	"N m-2"
	standard_name	"downward_x_stress_at_sea_water_surface"
	cell_methods	"area: mean where 3d ocean; time: monthly mean"
	comment	This is the zonal stress on the liquid ocean from overlying atmosphere, sea ice, ice shelf (expressed as a 2D variable) and possibly icebergs and any momentum flux correction.
tauvo	long_name	"Sea Water Downward Y Stress"
(time,lat,lon)	units	"N m-2"
	standard_name	"downward_y_stress_at_sea_water_surface"
	cell_methods	"area: mean where 3d ocean; time: monthly mean"
	comment	This is the meridional stress on the liquid ocean from overlying atmosphere, sea ice, ice shelf (expressed as a 2D variable) and possibly icebergs and any momentum flux correction.
msftbarot	long_name	"Ocean Barotropic Mass Streamfunction"
(time,lat,lon)	units	"kg s-1"
	standard_name	"ocean_barotropic_mass_streamfunction"
	cell_methods	"area: mean; time: monthly mean"
	comment	Quasi-barotropic streamfunction as discussed in appendix H26 of Griffies et al. (2016); for Boussinesq models, this is simply the volume barotropic streamfunction times the reference seawater volumic mass; the streamfunction Ψ is computed so that $\partial_y \Psi = U^\rho$ and $\partial_x \Psi = -V^\rho$, where U^ρ and V^ρ are the zonal and meridional vertically integrated velocities multiplied by seawater density (i.e., barotropic mass transports per distance along the section).
zos	long_name	"Sea Surface Height Above Geoid"
(time,lat,lon)	units	"m"
	standard_name	"sea_surface_height_above_geoid"
	cell_methods	"area: mean where 3d ocean; time: monthly mean"
	comment	This is the dynamic sea surface height above geoid, i.e. not including steric sea-level changes (see appendix H7 of Griffies et al., 2016).

Table A4. Continuation of Tab. A1

wfoat	long_name	"Water Mass Flux Into Sea Water From Atmosphere"
(time,lat,lon)	units	"kg m-2 s-1"
	positive	"downward"
	standard_name	
	cell_methods	"area: mean where 3d ocean; time: monthly mean"
	comment	This is calculated as condensation minus evaporation plus solid and liquid precipitation, only considering the part of these fluxes that enters the sea-ice free portion of the cell, but expressed per area of sea and sea-ice; considering appendix K2-K3 of Griffies et al. (2016), wfoat=pr+prsn+evs; models using virtual salt fluxes are invited to calculate an equivalent freshwater mass flux
flandice	long_name	"Water Mass Flux Into Sea Water From Land Ice"
(time,lat,lon)	units	"kg m-2 s-1"
	positive	"downward"
	standard_name	water_flux_into_sea_water_from_land_ice
	cell_methods	"area: mean where 3d ocean; time: monthly mean"
	comment	This is calculated as runoff from rivers or surface ice-sheet melting, plus iceberg melt, plus ice-shelf melt minus refreezing; considering appendix K2-K3 of Griffies et al. (2016), flandice=friver+ficeberg+ficeshelf; models using virtual salt fluxes are invited to calculate an equivalent freshwater mass flux
fsitherm	long_name	"Water Mass Flux Into Sea Water Due to Sea Ice Thermodynamics"
(time,lat,lon)	units	"kg m-2 s-1"
	positive	"downward"
	standard_name	"water_mass_flux_into_sea_water_due_to_sea_ice_thermodynamics"
	cell_methods	"area: mean where 3d ocean; time: monthly mean"
	comment	This is the net flux, calculated as sea-ice melt minus sea-ice formation/freezing; this is the flux into the total sea cell (open + sea-ice covered); models using virtual salt fluxes are invited to calculate an equivalent freshwater mass flux
wfocorr	long_name	"Water Mass Flux Into Sea Water From Salinity Correction"
(time,lat,lon)	units	"kg m-2 s-1"
	positive	"downward"
	standard_name	
	cell_methods	"area: mean where 3d ocean; time: monthly mean"
	comment	This is the flux corresponding to the sea surface salinity restoring/adjustment that is common in global ocean models; it should be set to zero for models with no correction; models using virtual salt fluxes are invited to calculate an equivalent freshwater mass flux; this variable is not officially part of CMIP6 but was used in OMIP

Table A5. Continuation of Tab. A1

hfs (time,lat,lon)	long_name	"Downward Heat Flux into Sea Water Surface"
	units	"W m-2"
	standard_name	
	cell_methods	"area: mean where 3d ocean; time: monthly mean"
	comment	This is calculated from the net shortwave and longwave radiative fluxes penetrating into the liquid water, the sensible and latent heat fluxes at the atmosphere–ocean, sea-ice–ocean, ice-shelf–ocean (expressed as a 2D variable) and iceberg–ocean interfaces, including those related to the heat content of runoff or precipitation, and any heat flux correction at the ocean surface; see list of individual fluxes in appendix K4 of Griffies et al. (2016); this variable is similar to the hfds variable in CMIP/OMIP, except that it includes potential heat flux correction
libmassbffl (time,lat,lon)	long_name	"Basal Specific Mass Balance of Floating Ice Shelf"
	units	"kg m-2 s-1"
	standard_name	"land_ice_basal_specific_mass_balance_flux"
	cell_methods	"area: mean where ice shelf; time: monthly mean"
	comment	This differs from the ficeshelf term in Griffies et al. (2016), which was the net water mass flux into sea water from ice shelf, i.e. per unit of ocean area, while libmassbffl is per unit of ice-shelf area; positive for melting, negative for refreezing
dydrflf (time,lat,lon)	long_name	"Dynamical Driving at the Base of Floating Ice Shelf"
	units	"m s-1"
	standard_name	
	cell_methods	"area: mean where ice shelf; time: monthly mean"
	comment	This is also referred to as the heat exchange velocity, i.e. friction velocity times heat exchange coefficient
thdrflf (time,lat,lon)	long_name	"Thermal Driving at the Base of Floating Ice Shelf"
	units	"degC"
	standard_name	
	cell_methods	"area: mean where ice shelf; time: monthly mean"
	comment	This is calculated as the potential temperature in the top ocean boundary layer beneath the ice shelf, minus the freezing potential temperature at the ice–ocean interface
hadrflf (time,lat,lon)	long_name	"Haline Driving at the Base of Floating Ice Shelf"
	units	"0.001"
	standard_name	
	cell_methods	"area: mean where ice shelf; time: monthly mean"
	comment	This is calculated as the practical salinity in the top ocean boundary layer beneath the ice shelf minus the salinity at the ice–ocean interface

Table A6. Continuation of Tab. A1

siconc	long_name	"Sea-Ice Area Percentage"
(time,lat,lon)	units	"%"
	standard_name	"sea_ice_area_fraction"
	cell_methods	"area: mean; time: monthly mean"
sivol	long_name	"Sea-Ice Volume per Area"
(time,lat,lon)	units	"m"
	standard_name	"sea_ice_thickness"
	cell_methods	"area: mean; time: monthly mean"
siu	long_name	"X-Component of the Sea-Ice Velocity"
(time,lat,lon)	units	"m s-1"
	standard_name	"sea_ice_x_velocity"
	cell_methods	"area: mean where sea ice; time: monthly mean"
	comment	Zonal velocity on the MISOMIP2 grid
siv	long_name	"Y-Component of the Sea-Ice Velocity"
(time,lat,lon)	units	"m s-1"
	standard_name	"sea_ice_y_velocity"
	cell_methods	"area: mean where sea ice; time: monthly mean"
	comment	Meridional velocity on the MISOMIP2 grid

Table A7. Global Attributes requested for the ocean outputs

Attribute name	Attribute value
project	'MISOMIP2'
contact	Name(s) of the person(s) who produced the simulation <email>
institute	Name of the institute(s) that produced the simulation (use '-' to separate multiple entities)
computing_facility	Computing center where the simulation was run
interpolation_method	e.g., 'linear triangular barycentric', 'bi-linear', 'nearest-neighbor', 'conservative'
ocean_model	Model name and version
reference	Main publication and/or website describing the simulation or a similar one, e.g. 'Naughten et al. (2021).'
original_sim_name	Original simulation name (so that each group keeps track of the one that was used in MISOMIP2), e.g. 'eORCA025.L121-OPM006'
experiment	MISOMIP2 experiment, e.g. 'OceanA-hind', 'IceOceanW-warm', ..
bathymetry	Bathymetry dataset (specify exact version), e.g. 'BedMachine-1.33', 'Bedmap2', 'RTopo-2.0.4', 'Merge of Millan et al. (2017) and Bedmap2'
ice_shelf_draft	Dataset for the depth of ice-shelf base (similar to previous).
atmosphere	Atmospheric forcing, with a reference, e.g., 'ERA5 (Hersbach et al. 2020)', 'ERAint (Dee et al. 2011)', 'JRA55do (Tsujino et al. 2018)', 'MARv3.9.3 (Donat-Magnin et al. 2020)'
iceberg	Method used to account for melting icebergs, with a reference, e.g. 'Lagrangian model (Martin and Adcroft 2010)', 'Prescribed freshwater (Merino et al. 2016)', 'Prescribed Freshwater and Heat (Merino et al. 2016)', 'None'
sea_ice	Method used to simulate or prescribe the ocean–sea-ice interaction, with a reference, e.g. 'Dynamics-Thermodynamics Model (Rousset et al. 2016)', 'Thermodynamics Model (Bitz and Lipscomb 1999)', 'Prescribed Freshwater and Heat'.
ocean_lateral_bdy	Type of lateral boundary conditions, e.g. 'Simulation (Merino et al. 2018)', 'Reanalysis (Mazloff et al. 2016)', 'Observations (Locarnini et al. 2018)', 'Corrected simulation (explain method)', 'None'.
tides	Method used to account for the effect of tides on ice-shelf melt, and dataset if relevant, e.g. 'Barotropic tidal harmonics prescribed at lateral boundaries (CATS)', 'Forced by a tidal potential', 'Parameterized through uniform tidal velocity in the three equations (utide=0.1 m s-1)', 'Parameterized through non-uniform tidal velocity in the three equations (FES2012)', 'None'.
vertical_coordinate	e.g. 'Geopotential (Z)', 'Stretched Geopotential (Zstar)', 'Pressure (P)', 'Stretched Pressure (P*)', 'Isopycnal', 'Terrain-Following (Sigma)', 'Arbitrary Lagrangian-Eulerian (ALE)'.
is_melt_param	Parameterization used to calculate ice-shelf basal melt rates, e.g. '3-equation (constant gamma)', '3-equation (velocity-dependent gamma)', '3-equation (stability and velocity-dependent gamma)'
eos	Equation of state, e.g. 'TEOS10', 'EOS80', 'linear'
advection	Brief description of the momentum- and tracer advection schemes (centered, third-order with limiter, etc.)

Table A8. Continuation of Tab. A7

horizontal_mixing	Brief description of how "horizontal" mixing was performed (harmonic, biharmonic, etc.; within model levels, along geopotentials, along isopycnals, etc.; using the Gent-McWilliams parameterisation; etc).
vertical_mixing	Brief description of how "vertical" mixing was performed (constant diffusivity, k-profile parameterisation, etc.; harmonic, biharmonic, etc).
convection	Brief description of the procedure for handling convection, e.g. 'Explicitly modeled', 'Parameterised using enhanced vertical mixing'.
avg_hor_res_73S	Average horizontal resolution (m) at 73°S in the MISOMIP2 domain (average of x and y resolution).
original_min_lat	Minimum latitude of the original domain, in [-90:90].
original_max_lat	Maximum latitude of the original domain, in [-90:90].
original_min_lon	Minimum longitude of the original domain, in [-180:180].
original_max_lon	Maximum longitude of the original domain, in [-180:180].

Table A9. Requested ice-sheet variables and their attributes. Variables that are modified or newly introduced in this article are underlined.

variable (dimensions)	attribute name	attribute value
x (x)	long_name	"X-coordinate"
	units	"m"
	axis	"X"
	comment	common MISOMIP2 grid
y (y)	long_name	"Y-coordinate"
	units	"m"
	axis	"Y"
	comment	common MISOMIP2 grid
time (time)	long_name	"time"
	units	"days since 1900-1-1 0:0:0" or "seconds since 1900-1-1 0:0:0", or since any other date.
	standard_name	"time"
	calendar	"standard", "no_leap", "360_day", or other specific year duration.
	bounds	"time_bounds"
	axis	"T"
	comment	The snapshots should correspond to 31st December of every years. The time_bounds variable should be defined with dimensions (time,bnds) to indicate the beginning and end of the years over which the yearly averages are done.
sftgif (x,y,time)	long_name	"Land Ice Area Percentage"
	units	"%"
	standard_name	"land_ice_area_fraction"
	cell_methods	"area: mean; time: instantaneous"
	comment	Land ice includes ice sheet, ice shelf, ice cap, glacier, not nunataks.
sftflf (x,y,time)	long_name	"Floating Ice Shelf Area Percentage"
	units	"%"
	standard_name	"floating_ice_shelf_area_fraction"
	cell_methods	"area: mean; time: instantaneous"
	comment	This does not include ice sheet fraction over subglacial lakes.
sftgrf (x,y,time)	long_name	"Grounded Ice Sheet Area Percentage"
	units	"%"
	standard_name	"grounded_ice_sheet_area_fraction"
	cell_methods	"area: mean; time: instantaneous"
	comment	This does not include ice shelves or ice sheet over subglacial lakes.

Table A10. Continuation of Fig. A9

lithk	long_name	"Ice Sheet Thickness"
(x,y,time)	units	"m"
	standard_name	"land_ice_thickness"
	cell_methods	"area: mean where land ice; time: instantaneous"
	comment	Physical thickness of the ice sheet, including air thickness from the firn layer if present
orog	long_name	"Ice Sheet Surface Altitude"
(x,y,time)	units	"m"
	standard_name	surface_altitude
	cell_methods	"area: mean where land ice; time: instantaneous"
	comment	The surface called 'surface' means the lower boundary of the atmosphere (top of ice shelf, ice sheet or firn layer if any). Altitude is the (geometric) height above the geoid, which is the reference geopotential surface. The geoid is similar to mean sea level.
base	long_name	"Ice Sheet Base Altitude"
(x,y,time)	units	"m"
	standard_name	base_altitude
	cell_methods	"area: mean where land ice; time: instantaneous"
	comment	Geometric height of the lower ice surface above the geoid; negative values correspond to a surface below mean sea level.
topg	long_name	"Bedrock Altitude"
(x,y,time)	units	"m"
	standard_name	"bedrock_altitude"
	cell_methods	"area: mean; time: instantaneous"
	comment	Calculated above geoid, i.e. negative values correspond to a surface below mean sea level; time dependency if glacial isostasy or adjustments are implemented.
rholi	long_name	"Depth Averaged Land Ice Density"
(x,y,time)	units	"kg m-3"
	standard_name	"ice_density"
	cell_methods	"area: mean where land ice; time: instantaneous"
	comment	Calculated as $\text{rholi} = \frac{1}{\text{lithk}} \int_{\text{base}}^{\text{orog}} \rho_i(z) \mathrm{d}z$, where ρ_i is the depth-dependent ice density.
tendlithk	long_name	"Tendency of Land Ice Thickness"
(x,y,time)	units	"m s-1"
	standard_name	
	cell_methods	"area: mean where land ice; time: yearly mean"
	comment	Ice thickness imbalance defined as $\text{tendlithk} = \frac{\mathrm{d}\,\text{lithk}}{\mathrm{d}t}$; introduced in MISOMIP2 to facilitate comparison to observations.

Table A11. Continuation of Fig. A9

acabf	long_name	"Surface Mass Balance Flux"
(x,y,time)	units	"kg m-2 s-1"
	standard_name	"land_ice_surface_specific_mass_balance_flux"
	cell_methods	"area: mean where land ice; time: yearly mean"
	comment	This is the net rate at which ice is added per unit area at the land ice surface due to all processes of surface accumulation (positive) and ablation (negative).
libmassbfgr	long_name	"Basal Specific Mass Balance Flux of Grounded Ice Sheet"
(x,y,time)	units	"kg m-2 s-1"
	standard_name	"land_ice_basal_specific_mass_balance_flux"
	cell_methods	"area: mean where grounded land ice; time: yearly mean"
	comment	This is the net rate at which ice is added per unit area at the base of grounded ice; positive for ice mass gain, negative for ice mass loss.
libmassbffl	long_name	"Basal Specific Mass Balance Flux of Floating Ice Shelf"
(x,y,time)	units	"kg m-2 s-1"
	standard_name	"land_ice_basal_specific_mass_balance_flux"
	cell_methods	"area: mean where ice shelf; time: yearly mean"
	comment	This is the net rate at which ice is added per unit area at the base of ice shelves; positive for ice mass gain (refreezing), negative for ice mass loss (melting).
licalvf	long_name	"Land Ice Calving Flux"
(x,y,time)	units	"kg m-2 s-1"
	standard_name	"land_ice_specific_mass_flux_due_to_calving"
	cell_methods	"area: mean where land ice; time: yearly mean"
	comment	Calculated as the rate of mass loss by the ice sheet (in kg s-1) divided by the horizontal area (m2) of the ice sheet grid box where calving occurred. Only for grid cells in contact with ocean.
ligroundf	long_name	"Land Ice Flux across the Grounding Line"
(x,y,time)	units	"kg m-2 s-1"
	standard_name	$grounding_line_flux$
	cell_methods	"area: mean where grounded ice; time: yearly mean"
	comment	Loss of grounded ice mass resulting at grounding line. Only for grid cells in contact with grounding line.

Table A12. Continuation of Fig. A9

xvelmean	long_name	"X-Component of Land Ice Vertical Mean Velocity"
(x,y,time)	units	"m s-1"
	standard_name	"land_ice_vertical_mean_x_velocity"
	cell_methods	"area: mean where land ice; time: yearly mean"
	comment	Averaged from the bedrock to the ice surface.
yvelmean	long_name	"Y-Component of Land Ice Vertical Mean Velocity"
(x,y,time)	units	"m s-1"
	standard_name	"land_ice_vertical_mean_y_velocity"
	cell_methods	"area: mean where land ice; time: yearly mean"
	comment	Averaged from the bedrock to the ice surface.
xvelsurf	long_name	"X-Component of Land Ice Surface Velocity"
(x,y,time)	units	"m s-1"
	standard_name	"land_ice_surface_x_velocity"
	cell_methods	"area: mean where land ice; time: yearly mean"
	comment	This is equal to xvelmean in 1-layer ice sheet models.
yvelsurf	long_name	"Y-Component of Land Ice Surface Velocity"
(x,y,time)	units	"m s-1"
	standard_name	"land_ice_surface_y_velocity"
	cell_methods	"area: mean where land ice; time: yearly mean"
	comment	This is equal to yvelmean in 1-layer ice sheet models.
strbasemag	long_name	"Land Ice Basal Drag"
(x,y,time)	units	"Pa" or "N m-2"
	standard_name	"land_ice_basal_drag"
	cell_methods	"area: mean where land ice; time: yearly mean"
	comment	This is the magnitude of the tangential basal traction opposing the ice flow.

Table A13. Global attributes requested for the ice outputs

Attribute name	Attribute value
project	'MISOMIP2'
contact	Name(s) of the person(s) who produced the simulation <email>
institute	Name of the institute(s) that produced the simulation (use "-" to separate multiple entities).
computing_facility	Computing center where the simulation was run.
interpolation_method	e.g., 'linear triangular barycentric', 'bi-linear', 'nearest-neighbor', 'conservative'.
ice_sheet_model	Model name and version
reference	Main publication or website describing the simulation or a similar one.
original_sim_name	Original simulation name (if applicable, so that each group keeps track of the one that was used in MISOMIP2).
experiment	MISOMIP2 experiment, e.g. 'IceOceanA-hind', 'IceOceanW-warm', ..
bedrock	Bedrock/bathymetry dataset (specify exact version), e.g. 'BedMachine-1.33', 'Bedmap2', 'RTopo-2.0.4', 'Merge of Millan et al. (2017) and Bedmap2'.
surface_mass_balance	Surface Mass Balance forcing, with a reference, e.g., 'MARv10 (Kittel et al. 2022)', 'ERAint (Dee et al. 2011)'
basal_mass_balance	Method, parameter, and input data used to calculate the ice shelf basal mass balance, e.g., 'ISMIP6 standard MeanAnt and ISMIP6 data (Jourdain et al. 2020)', 'PICO (Reese et al. 2018), calibration from Reese et al. (2022) and ocean data from Schmidtko et al. (2014).'
initialization	Method used to initialize the ice sheet model, e.g., '1000-year spin up under pre-industrial conditions', 'Inversion of ice-sheet surface velocities and surface elevation for the mid 1990s followed by a 10-year relaxation'.
basal_friction	Type of basal friction and reference, e.g., 'Non-linear (Weertman 1957)', 'Based on effective pressure (Tsai et al. 2015)'.
ice_flow_equation	e.g., 'Shallow Shelf Approximation (MacAyeal 1989)', 'Full Stokes equation'
rheology	Provide information such as the exponent in Glen's law, the enhancement factor, whether temperature or damage are considered in the ice effective viscosity, etc.
calving	Method used to represent calving and reference, e.g., 'Fixed calving front', etc.
avg_GL_res	Average horizontal resolution (m) of the original grid along the grounding line.
coupling_method	Reference or description of the ice-shelf–ocean coupling method, e.g., 'Favier et al. (2019)', 'Goldberg et al. (2018)'.
coupling_period	e.g., '1 year', '1450 s (ocean model time step)'.

41

References

Adusumilli, S., Fricker, H. A., Medley, B., Padman, L., and Siegfried, M. R.: Interannual variations in meltwater input to the Southern Ocean from Antarctic ice shelves, Nature Geoscience, 13, 616–620, https://doi.org/10.1038/s41561-020-0616-z, 2020.

Asay-Davis, X. S., Cornford, S. L., Durand, G., Galton-Fenzi, B. K., Gladstone, R. M., Gudmundsson, G. H., Hattermann, T., Holland, D. M., Holland, D., Holland, P. R., et al.: Experimental design for three interrelated Marine Ice-Sheet and Ocean Model Intercomparison Projects, Geosci. Model Dev., 9, 2471–2497, https://doi.org/10.5194/gmd-9-2471-2016, 2016.

Bamber, J. L., Riva, R. E. M., Vermeersen, B. L. A., and LeBrocq, A. M.: Reassessment of the potential sea-level rise from a collapse of the West Antarctic Ice Sheet, Science, 324, 901–903, https://doi.org/10.1126/science.1169335, 2009.

Bett, D. T., Bradley, A. T., Williams, C. R., Holland, P. R., Arthern, R. J., and Goldberg, D. N.: Coupled ice/ocean interactions during the future retreat of West Antarctic ice streams, The Cryosphere Discussions, 2023, 1–28, https://doi.org/10.5194/tc-2023-77, 2023.

Bevan, S., Cornford, S., Gilbert, L., Otosaka, I., Martin, D., and Surawy-Stepney, T.: Amundsen Sea Embayment ice-sheet mass-loss predictions to 2050 calibrated using observations of velocity and elevation change, Journal of Glaciology, p. 1–11, https://doi.org/10.1017/jog.2023.57, 2023.

Boucher, O., Servonnat, J., Albright, A. L., Aumont, O., Balkanski, Y., Bastrikov, V., Bekki, S., Bonnet, R., Bony, S., Bopp, L., et al.: Presentation and evaluation of the IPSL-CM6A-LR climate model, J. Adv. Model. Ea. Sys., 12, https://doi.org/10.1029/2019MS002010, 2020.

Burgard, C., Jourdain, N. C., Reese, R., Jenkins, A., and Mathiot, P.: An assessment of basal melt parameterisations for Antarctic ice shelves, The Cryosphere, 0, 1–56, https://doi.org/10.5194/tc-16-4931-2022, 2022.

Comeau, D., Asay-Davis, X. S., Begeman, C. B., Hoffman, M. J., Lin, W., Petersen, M. R., Price, S. F., Roberts, A. F., Van Roekel, L. P., Veneziani, M., Wolfe, J. D., Fyke, J. G., Ringler, T. D., and Turner, A. K.: The DOE E3SM v1. 2 Cryosphere Configuration: Description and Simulated Antarctic Ice-Shelf Basal Melting, J. Adv. Model. Ea. Sys., 14, https://doi.org/10.1029/2021MS002468, 2022.

Cornford, S. L., Seroussi, H., Asay-Davis, X. S., Gudmundsson, G. H., Arthern, R., Borstad, C., Christmann, J., Dias dos Santos, T., Feldmann, J., Goldberg, D., et al.: Results of the third Marine Ice Sheet Model Intercomparison Project (MISMIP+), The Cryosphere, 14, 2283–2301, https://doi.org/10.5194/tc-14-2283-2020, 2020.

Davis, P. E., Nicholls, K. W., Holland, D. M., Schmidt, B. E., Washam, P., Riverman, K. L., Arthern, R. J., Vaňková, I., Eayrs, C., Smith, J. A., et al.: Suppressed basal melting in the eastern Thwaites Glacier grounding zone, Nature, 614, 479–485, https://doi.org/10.1038/s41586-022-05586-0, 2023.

Davis, P. E. D., Nicholls, K. W., and Holland, D.: Thwaites MELT: Temperature, salinity and velocity time series from the grounding zone region of Thwaites Glacier Eastern ice shelf (2020) (Version 1.0) [Data set], Tech. rep., UK Polar Data Centre, Natural Environment Research Council, UK Research Innovation, https://doi.org/10.5285/4ffad557-1c3c-4ea7-a73d-6d782331b08a, 2021.

De Rydt, J. and Gudmundsson, G. H.: Coupled ice shelf-ocean modeling and complex grounding line retreat from a seabed ridge, J. Geophys. Res., 121, 865–880, https://doi.org/10.1002/2015JF003791, 2016.

De Rydt, J. and Naughten, K.: Geometric amplification and suppression of ice-shelf basal melt in West Antarctica, The Cryosphere, 18, 1863–1888, https://doi.org/10.5194/tc-18-1863-2024, 2024.

Dutrieux, P., De Rydt, J., Jenkins, A., Holland, P. R., Ha, H. K., Lee, S. H., Steig, E. J., Ding, Q., Abrahamsen, E. P., and Schröder, M.: Strong sensitivity of Pine Island ice-shelf melting to climatic variability, Science, 343, 174–178, https://doi.org/10.1126/science.1244341, 2014.

735   Fahrbach, E. and Rohardt, G.: Physical oceanography during POLARSTERN cruise ANT-VIII/2 (WWGS) on section SR02 and SR04, PANGAEA, https://doi.org/10.1594/PANGAEA.742580, in supplement to: Hellmer, Hartmut H; Huhn, Oliver; Gomis, Damià; Timmermann, Ralph (2011): On the freshening of the northwestern Weddell Sea continental shelf. Ocean Science, 7(3), 305-316, https://doi.org/10.5194/os-7-305-2011, 1990.

Fahrbach, E. and Rohardt, G.: Physical oceanography during POLARSTERN cruise ANT-IX/2 on section SR04, PANGAEA,
740   https://doi.org/10.1594/PANGAEA.735277, in supplement to: Hellmer, Hartmut H; Huhn, Oliver; Gomis, Damià; Timmermann, Ralph (2011): On the freshening of the northwestern Weddell Sea continental shelf. Ocean Science, 7(3), 305-316, https://doi.org/10.5194/os-7-305-2011, 1991.

Fahrbach, E. and Rohardt, G.: Physical oceanography during POLARSTERN cruise ANT-X/7 on section SR04, PANGAEA, https://doi.org/10.1594/PANGAEA.742651, in supplement to: Hellmer, Hartmut H; Huhn, Oliver; Gomis, Damià; Timmermann, Ralph
745   (2011): On the freshening of the northwestern Weddell Sea continental shelf. Ocean Science, 7(3), 305-316, https://doi.org/10.5194/os-7-305-2011, 1993.

Fahrbach, E. and Rohardt, G.: Physical oceanography during POLARSTERN cruise ANT-XIII/4 on section S04A, PANGAEA, https://doi.org/10.1594/PANGAEA.738489, in supplement to: Hellmer, Hartmut H; Huhn, Oliver; Gomis, Damià; Timmermann, Ralph (2011): On the freshening of the northwestern Weddell Sea continental shelf. Ocean Science, 7(3), 305-316, https://doi.org/10.5194/os-7-
750   305-2011, 1996.

Fahrbach, E. and Rohardt, G.: Physical oceanography during POLARSTERN cruise ANT-XV/4 (DOVETAIL) on section SR04, PANGAEA, https://doi.org/10.1594/PANGAEA.742626, in supplement to: Hellmer, Hartmut H; Huhn, Oliver; Gomis, Damià; Timmermann, Ralph (2011): On the freshening of the northwestern Weddell Sea continental shelf. Ocean Science, 7(3), 305-316, https://doi.org/10.5194/os-7-305-2011, 1998.

755   Fahrbach, E. and Rohardt, G.: Physical oceanography during POLARSTERN cruise ANT-XXIV/3, PANGAEA, https://doi.org/10.1594/PANGAEA.733414, in supplement to: Hellmer, Hartmut H; Huhn, Oliver; Gomis, Damià; Timmermann, Ralph (2011): On the freshening of the northwestern Weddell Sea continental shelf. Ocean Science, 7(3), 305-316, https://doi.org/10.5194/os-7-305-2011, 2008.

Favier, L., Jourdain, N. C., Jenkins, A., Merino, N., Durand, G., Gagliardini, O., Gillet-Chaulet, F., and Mathiot, P.: Assessment of Sub-
760   Shelf Melting Parameterisations Using the Ocean-Ice Sheet Coupled Model NEMO (v3. 6)-Elmer/Ice (v8. 3), Geosci. Model Dev., https://doi.org/10.5194/gmd-12-2255-2019, 2019.

Foldvik, A., Gammelsrød, T., and Tørresen, T.: Hydrographic observations from the Weddell Sea during the Norwegian Antarctic Research Expedition 1976/77, Polar Research, 3, 177–193, https://doi.org/10.1111/j.1751-8369.1985.tb00506.x, 1985.

Gardner, A., Fahnestock, M., and Scambos, T.: MEaSUREs ITS_LIVE Regional Glacier and Ice Sheet Surface Velocities, Version 1,
765   https://doi.org/10.5067/6II6VW8LLWJ7, 2022.

Gohl, K.: Station list and links to master tracks in different resolutions of POLARSTERN cruise ANT-XXVI/3, Wellington - Punta Arenas, 2010-01-30 - 2010-04-05, Tech. rep., Alfred Wegener Institute, Helmholtz Centre for Polar and Marine Research, Bremerhaven, https://doi.org/10.1594/PANGAEA.847944, 2015.

Gohl, K.: The Expedition PS104 of the Research Vessel POLARSTERN to the Amundsen Sea in 2017, Reports on polar and marine research,
770   Tech. rep., Alfred Wegener Institute for Polar and Marine Research, Bremerhaven, https://doi.org/10.2312/BzPM_0712_2017, 2017.

Goldberg, D. N., Snow, K., Holland, P., Jordan, J. R., Campin, J.-M., Heimbach, P., Arthern, R., and Jenkins, A.: Representing grounding line migration in synchronous coupling between a marine ice sheet model and a z-coordinate ocean model, Ocean Model., 125, 45–60, https://doi.org/10.1016/j.ocemod.2018.03.005, 2018.

Griffies, S. M., Danabasoglu, G., Durack, P. J., Adcroft, A. J., Balaji, V., Böning, C. W., Chassignet, E. P., Curchitser, E., Deshayes, J., Drange, H., et al.: OMIP contribution to CMIP6: Experimental and diagnostic protocol for the physical component of the Ocean Model Intercomparison Project, Geoscientific Model Development, 9, 3231–3296, https://doi.org/10.5194/gmd-9-3231-2016, 2016.

Gwyther, D. E., Galton-Fenzi, B. K., Dinniman, M. S., Roberts, J. L., and Hunter, J. R.: The effect of basal friction on melting and freezing in ice shelf–ocean models, Ocean Model., 95, 38–52, https://doi.org/10.1016/j.ocemod.2015.09.004, 2015.

Gwyther, D. E., Kusahara, K., Asay-Davis, X. S., Dinniman, M. S., and Galton-Fenzi, B. K.: Vertical processes and resolution impact ice shelf basal melting: A multi-model study, Ocean Model., 147, 101 569, https://doi.org/10.1016/j.ocemod.2020.101569, 2020.

Hattermann, T., Nicholls, K. W., Hellmer, H. H., Davis, P. E., Janout, M. A., Østerhus, S., Schlosser, E., Rohardt, G., and Kanzow, T.: Observed interannual changes beneath Filchner-Ronne Ice Shelf linked to large-scale atmospheric circulation, Nature communications, 12, 2961, https://doi.org/10.1038/s41467-021-23131-x, 2021.

Hazel, J. E. and Stewart, A. L.: Bistability of the Filchner-Ronne Ice Shelf Cavity Circulation and Basal Melt, J. Geophys. Res. Oceans, 125, e2019JC015 848, https://doi.org/10.1029/2019JC015848, 2020.

Hellmer, H. H., Kauker, F., Timmermann, R., and Hattermann, T.: The fate of the southern Weddell Sea continental shelf in a warming climate, J. Climate, 30, 4337–4350, https://doi.org/10.1175/JCLI-D-16-0420.1, 2017.

Heywood, K. J.: JR294/295 Cruise Report, Ice Sheet Stability Programme (iSTAR), RRS James Clark Ross, 26th February – 8th March 2014, Amundsen Sea, Tech. rep., Natural Environment Research Council (NERC), https://www.bodc.ac.uk/resources/inventories/cruise_inventory/report/13405/, 2014.

Heywood, K. J., Biddle, L. C., Boehme, L., Dutrieux, P., Fedak, M., Jenkins, A., Jones, R. W., Kaiser, J., Mallett, H., et al.: Between the devil and the deep blue sea: the role of the Amundsen Sea continental shelf in exchanges between ocean and ice shelves, Oceanography, 29, 118–129, https://doi.org/10.5670/oceanog.2016.104, 2016.

Holland, D., Hunter, J., Grosfeld, K., Hellmer, H., Jenkins, A., Morales Maqueda, M., Hemer, M., Williams, M., Klinck, J., and Dinniman, M.: The ice shelf-ocean model intercomparison project (ISOMIP), in: Eos Trans. AGU, 84, Fall Meet. Suppl., vol. 2003, pp. C41A–05, 2003.

Holland, P. R., Bevan, S. L., and Luckman, A. J.: Strong Ocean Melting Feedback During the Recent Retreat of Thwaites Glacier, Geophysical Research Letters, 50, https://doi.org/10.1029/2023GL103088, 2023.

Hubold, G., and Drescher, H. E.: Die Filchner-Schelfeis-Expedition 1980/81 mit MS "Polarsirkel". Liste der Planktonfänge und Lichtstärkemessungen, https://epic.awi.de/id/eprint/26181/1/BerPolarforsch19824.pdf, 1982.

Hunter, J. R.: Specification for Test Models of Ice Shelf Cavities, Tech. rep., Antarctic Climate & Ecosystems Cooperative Research Centre, Hobart, Tasmania, https://www.johnroberthunter.org/science/home_prof/reports/test_cavities.pdf, 2006.

IOC, SCOR, and IAPSO: The international thermodynamic equation of seawater - 2010 : Calculation and use of thermodynamic properties, Tech. rep., Intergovernmental Oceanographic Commission, http://www.teos-10.org/pubs/TEOS-10_Manual.pdf, 2010.

Jacobs, S.: Cruise NBP9402, RVIB Nathaniel B. Palmer, Feb 14 – Apr 5 1994, Tech. rep., United States Antarctic Program, https://doi.org/10.7284/905397, 1994.

Jacobs, S.: Cruise NBP0001, RVIB Nathaniel B. Palmer, Feb 15 – Apr 1 2000, Tech. rep., United States Antarctic Program, https://doi.org/10.7284/905450, 2000.

Jacobs, S.: Cruise NBP0702, RVIB Nathaniel B. Palmer, Feb 03 – Mar 25 2007, Tech. rep., United States Antarctic Program, https://doi.org/10.7284/905530, 2007.

Jacobs, S.: Cruise NBP0901, RVIB Nathaniel B. Palmer, Jan 05 – Feb 26 2009, Tech. rep., United States Antarctic Program, https://doi.org/10.7284/905547, 2009.

Jacobs, S., Giulivi, C., Dutrieux, P., Rignot, E., Nitsche, F., and Mouginot, J.: Getz Ice Shelf melting response to changes in ocean forcing, J. Geophys. Res., 118, 4152–4168, https://doi.org/10.1002/jgrc.20298, 2013.

Janout, M. A., Hellmer, H. H., Schröder, M., and Wisotzki, A.: Physical oceanography during POLARSTERN cruise PS111 (ANT-XXXIII/2), https://doi.org/10.1594/PANGAEA.897280, 2019.

Jenkins, A., Shoosmith, D., Dutrieux, P., Jacobs, S., Kim, T. W., Lee, S. H., Ha, H. K., and Stammerjohn, S.: West Antarctic Ice Sheet retreat in the Amundsen Sea driven by decadal oceanic variability, Nature Geosc., 11, 733–738, 2018.

Joughin, I., Shapero, D., Smith, B., Dutrieux, P., and Barham, M.: Ice-shelf retreat drives recent Pine Island Glacier speedup, Science Advances, 7, eabg3080, https://doi.org/10.1126/sciadv.abg3080, 2021.

Jourdain, N. C., Asay-Davis, X., Hattermann, T., Straneo, F., Seroussi, H., Little, C. M., and Nowicki, S.: A protocol for calculating basal melt rates in the ISMIP6 Antarctic ice sheet projections, The Cryosphere, 14, 3111–3134, https://doi.org/10.5194/tc-14-3111-2020, 2020.

Jourdain, N. C., Mathiot, P., Burgard, C., Caillet, J., and Kittel, C.: Ice shelf basal melt rates in the Amundsen Sea at the end of the 21st century, Geophys. Res. Lett., https://doi.org/10.1029/2022GL100629, 2022.

Kim, T. W., H, H. K., and Hong, C. S.: The Amundsen Sea Expedition (ANA02C): IBRV Araon, 31 January 2012 – 20 March 2012 – Chapter 1: Hydrographic Survey, Tech. rep., Korea Polar Research Institute, Incheon, https://repository.kopri.re.kr/handle/201206/4603, 2012.

Kim, T. W., Cho, K. H., Kim, C. S., Yang, H. W., La, H. S., Lee, J. H., Kim, D. K., Jung, J. H., Wåhlin, A. K., Assmann, K. M., Darelius, E., Abrahamsen, E. P., and Waite, N.: The Amundsen Sea Expedition (ANA06B): IBRV Araon, 6 January – 23 February 2016 – Chapter 1: Physical Oceanography in Amundsen Sea, Tech. rep., Korea Polar Research Institute, Incheon, https://ftp.nmdc.no/nmdc/UIB/Mooring/20181213/ANA06B_cruise_report.pdf, 2016.

Kim, T.-W., Ha, H. K., Wåhlin, A. K., Lee, S., Kim, C.-S., Lee, J. H., and Cho, Y.-K.: Is Ekman pumping responsible for the seasonal variation of warm circumpolar deep water in the Amundsen Sea?, Continental Shelf Research, 132, 38–48, https://doi.org/10.1016/j.csr.2016.09.005, 2017.

Kim, T. W., Cho, K. H., Park, T. W., Yang, H. W., Kim, Y., Assmann, K. M., Rolandsson, J., Dutrieux, P., Gobat, J., Beem, L., Richter, T., Buhl, D., and Durand, I.: The Amundsen Sea Expedition (ANA08B): IBRV Araon, 21 December 2017 – 13 February 2018 – Chapter 1: Physical Oceanography, Tech. rep., Korea Polar Research Institute, Incheon, https://repository.kopri.re.kr/handle/201206/9441, 2018.

Kreuzer, M., Reese, R., Huiskamp, W. N., Petri, S., Albrecht, T., Feulner, G., and Winkelmann, R.: Coupling framework (1.0) for the PISM (1.1. 4) ice sheet model and the MOM5 (5.1. 0) ocean model via the PICO ice shelf cavity model in an Antarctic domain, Geosci. Mod. Dev., 14, 3697–3714, https://doi.org/10.5194/gmd-14-3697-2021, 2021.

Larter, R., Barham, M., Boehme, L., Braddock, S., Graham, A., Hogan, K., Mazur, A., Minzoni, R., Queste, B., Sheehan, P., Spoth, M., Wåhlin, A., Bortolotto-d'Oliveira, G., Clark, R. W., Fitzgerald, V., Karam, S., Kirkham, J., Stedt, F., Zheng, Y., Beeler, C., Goodell, J., Rush, E., Snow, T., Welzenbach, L., Andersson, J., and Rolandsson, J.: Cruise NBP1902, RVIB Nathaniel B. Palmer, Jan 29 – Mar 25 2019, Tech. rep., United States Antarctic Program, https://doi.org/10.7284/908147, 2019.

845 Locarnini, R. A., Mishonov, A. V., Baranova, O. K., Boyer, T. P., Zweng, M. M., Garcia, H. E., Reagan, J. R., Seidov, D., Weathers, K. W., Paver, C. R., and Smolyar, I. V.: World Ocean Atlas 2018, Volume 1: Temperature, Tech. Rep. Atlas NESDIS 81, NOAA, https://data.nodc.noaa.gov/woa/WOA18/DOC/woa18_vol1.pdf, 2019.

Losch, M.: Modeling ice shelf cavities in az coordinate ocean general circulation model, J. Geophys. Res., 113, https://doi.org/10.1029/2007JC004368, 2008.

850 Lurton, T., Balkanski, Y., Bastrikov, V., Bekki, S., Bopp, L., Braconnot, P., Brockmann, P., Cadule, P., Contoux, C., Cozic, A., et al.: Implementation of the CMIP6 Forcing Data in the IPSL-CM6A-LR Model, J. Adv. Model. Ea. Sys., 12, https://doi.org/10.1029/2019MS001940, 2020.

Mathiot, P. and Jourdain, N. C.: Southern Ocean warming and Antarctic ice shelf melting in conditions plausible by late 23rd century in a high-end scenario, Ocean Science, 19, 1595–1615, https://doi.org/10.5194/os-19-1595-2023, 2023.

855 Mathiot, P., Jenkins, A., Harris, C., and Madec, G.: Explicit and parametrised representation of under ice shelf seas in the z* coordinate ocean model NEMO 3.6, Geosci. Model Dev., 10, 2849–2874, https://doi.org/10.5194/gmd-10-2849-2017, 2017.

Meinshausen, M., Nicholls, Z. R. J., Lewis, J., Gidden, M. J., Vogel, E., Freund, M., Beyerle, U., Gessner, C., Nauels, A., Bauer, N., et al.: The shared socio-economic pathway (SSP) greenhouse gas concentrations and their extensions to 2500, Geosci. Model Dev., 13, 3571–3605, https://doi.org/10.5194/gmd-13-3571-2020, 2020.

860 Milillo, P., Rignot, E., Rizzoli, P., Scheuchl, B., Mouginot, J., Bueso-Bello, J., and Prats-Iraola, P.: Heterogeneous retreat and ice melt of Thwaites Glacier, West Antarctica, Science Advances, 5, eaau3433, https://doi.org/10.1126/sciadv.aau3433, 2019.

Milillo, P., Rignot, E., Rizzoli, P., Scheuchl, B., Mouginot, J., Bueso-Bello, J. L., Prats-Iraola, P., and Dini, L.: Rapid glacier retreat rates observed in West Antarctica, Nature Geoscience, 15, 48–53, https://doi.org/10.1038/s41561-021-00877-z, 2022.

Moholdt, G., Padman, L., and Fricker, H. A.: Basal mass budget of Ross and Filchner-Ronne ice shelves, Antarctica, derived from Lagrangian
865 analysis of ICESat altimetry, J. Geophys. Res., 119, 2361–2380, https://doi.org/10.1002/2014JF003171, 2014.

Morlighem, M.: MEaSUREs BedMachine Antarctica, Version 3, Tech. rep., Boulder, Colorado USA. NASA National Snow and Ice Data Center Distributed Active Archive Center, https://doi.org/10.5067/FPSU0V1MWUB6, https://doi.org/10.5067/FPSU0V1MWUB6, 2022.

Mouginot, J., Scheuchl, B., and Rignot, E.: MEaSUREs Annual Antarctic Ice Velocity Maps, Version 1, https://doi.org/10.5067/9T4EPQXTJYW9, 2017a.

870 Mouginot, J., Scheuchl, B., and Rignot, E.: MEaSUREs Antarctic Boundaries for IPY 2007-2009 from Satellite Radar, Version 2, Tech. rep., Boulder, Colorado USA. NASA National Snow and Ice Data Center Distributed Active Archive Center, https://doi.org/10.5067/AXE4121732AD, 2017b.

Nakayama, Y., Schröder, M., and Hellmer, H. H.: From circumpolar deep water to the glacial meltwater plume on the eastern Amundsen Shelf, Deep Sea Res. I, 77, 50–62, https://doi.org/10.1016/j.dsr.2013.04.001, 2013.

875 Nakayama, Y., Cai, C., and Seroussi, H.: Impact of subglacial freshwater discharge on Pine Island Ice Shelf, Geophys. Res. Lett., 48, https://doi.org/10.1029/2021GL093923, 2021.

Naughten, K. A., De Rydt, J., Rosier, S. H. R., Jenkins, A., Holland, P. R., and Ridley, J. K.: Two-timescale response of a large Antarctic ice shelf to climate change, Nature Comm., 12, 1–10, https://doi.org/10.1038/s41467-021-22259-0, 2021.

Naughten, K. A., Holland, P. R., Dutrieux, P., Kimura, S., Bett, D. T., and Jenkins, A.: Simulated twentieth-century ocean warming in the
880 Amundsen Sea, West Antarctica, Geophys. Res. Lett., 49, https://doi.org/10.1029/2021GL094566, 2022.

Naughten, K. A., Holland, P. R., and Rydt, J. D.: Unavoidable future increase in West Antarctic ice-shelf melting over the twenty-first century, Nature Climate Change, https://doi.org/10.1038/s41558-023-01818-x, 2023.

Nicholls, K. W., Østerhus, S., Makinson, K., Gammelsrød, T., and Fahrbach, E.: Ice-ocean processes over the continental shelf of the southern Weddell Sea, Antarctica: A review, Reviews of Geophysics, 47, https://doi.org/10.1029/2007RG000250, 2009.

885   Nilsson, J., Gardner, A. S., and Paolo, F. S.: MEaSUREs ITS_LIVE Antarctic Grounded Ice Sheet Elevation Change, Version 1, https://doi.org/10.5067/L3LSVDZS15ZV, 2023.

Nowicki, S., Payne, A., Goelzer, H., Seroussi, H., Lipscomb, W., Abe-Ouchi, A., Agosta, C., Alexander, P., Asay-Davis, X., Barthel, A., Bracegirdle, T., Cullather, R., Felikson, D., Fettweis, X., Gregory, J., Hatterman, T., Jourdain, N., C., Kuipers Munneke, P., Larour, E., Little, C., Morlinghem, M., Nias, I., Shepherd, A., Simon, E., Slater, D., Smith, R., Straneo, F., Trusel, L., van den Broeke, M., and van de

890   Wal, R.: Experimental protocol for sea level projections from ISMIP6 standalone ice sheet models, The Cryosphere, 14, 2331–2368, https://doi.org/10.5194/tc-14-2331-2020, 2020.

Nowicki, S. M. J., Payne, A., Larour, E., Seroussi, H., Goelzer, H., Lipscomb, W., Gregory, J., Abe-Ouchi, A., and Shepherd, A.: Ice Sheet Model Intercomparison Project (ISMIP6) contribution to CMIP6, Geosci. Model Dev., 9, 4521, https://doi.org/10.5194/gmd-9-4521-2016, 2016.

895   Otosaka, I., Gilbert, L., and Shepherd, A.: Surface elevation change of the Amundsen Sea Embayment 1992-2019, https://doi.org/10.5281/zenodo.8117577, 2023.

Paolo, F. S., Gardner, A. S., Greene, C. A., Nilsson, J., Schodlok, M. P., Schlegel, N.-J., and Fricker, H. A.: Widespread slowdown in thinning rates of West Antarctic ice shelves, The Cryosphere, 17, 3409–3433, https://doi.org/10.5194/tc-17-3409-2023, 2023a.

Paolo, F. S., Gardner, A. S., Greene, C. A., and Schlegel, N.-J.: MEaSUREs ITS_LIVE Antarctic Ice Shelf Height Change and Basal Melt

900   Rates, Version 1, https://doi.org/10.5067/SE3XH9RXQWAM, 2023b.

Pattyn, F.: The paradigm shift in Antarctic ice sheet modelling, Nature Comm., 9, 1–3, https://doi.org/10.1038/s41467-018-05003-z, 2018.

Pattyn, F., Schoof, C., Perichon, L., Hindmarsh, R. C. A., Bueler, E., de Fleurian, B., Durand, G., Gagliardini, O., Gladstone, R., Goldberg, D., et al.: Results of the marine ice sheet model intercomparison project, MISMIP, The Cryosphere, 6, 573–588, https://doi.org/10.5194/tc-6-573-2012, 2012.

905   Pattyn, F., Perichon, L., Durand, G., Favier, L., Gagliardini, O., Hindmarsh, R. C. A., Zwinger, T., Albrecht, T., Cornford, S. L., Docquier, D., Fürst, J. J., Goldberg, D., Gudmundsson, G. H., Humbert, A., Hütten, M., Huybrechts, P., Jouvet, G., Kleiner, T., Larour, E., Martin, D., Morlighem, M., Payne, A. J., Pollard, D., Rückamp, M., Rybak, O., Seroussi, H., Thoma, M., and Wilkens, N.: Grounding-line migration in plan-view marine ice-sheet models: results of the ice2sea MISMIP3d intercomparison, J. Glaciology, 59, 410–422, https://doi.org/10.3189/2013JoG12J129, 2013.

910   Payne, A. J., Nowicki, S., Abe-Ouchi, A., Agosta, C., Alexander, P., Albrecht, T., Asay-Davis, X., Aschwanden, A., Barthel, A., Bracegirdle, T. J., et al.: Future sea level change under CMIP5 and CMIP6 scenarios from the Greenland and Antarctic ice sheets, Geophysical Research Letters, https://doi.org/10.1029/2020GL091741, 2021.

Pelle, T., Morlighem, M., Nakayama, Y., and Seroussi, H.: Widespread grounding line retreat of Totten Glacier, East Antarctica, over the 21st century, Geophysical Research Letters, 48, https://doi.org/10.1029/2021GL093213, 2021.

915   Pelletier, C., Fichefet, T., Goosse, H., Haubner, K., Helsen, S., Huot, P.-V., Kittel, C., Klein, F., Le clec'h, S., van Lipzig, N. P. M., Marchi, S., Massonnet, F., Mathiot, P., Moravveji, E., Moreno-Chamarro, E., Ortega, P., Pattyn, F., Souverijns, N., Van Achter, G., Vanden Broucke, S., Vanhulle, A., Verfaillie, D., and Zipf, L.: PARASO, a circum-Antarctic fully coupled ice-sheet–ocean–sea-ice–atmosphere–land model involving f.ETISh1.7, NEMO3.6, LIM3.6, COSMO5.0 and CLM4.5, Geosci. Mod. Dev., 15, 553–594, https://doi.org/10.5194/gmd-15-553-2022, 2022.

920 Reese, R., Garbe, J., Hill, E. A., Urruty, B., Naughten, K. A., Gagliardini, O., Durand, G., Gillet-Chaulet, F., Gudmundsson, G. H., Chandler, D., Langebroek, P. M., and Winkelmann, R.: The stability of present-day Antarctic grounding lines – Part 2: Onset of irreversible retreat of Amundsen Sea glaciers under current climate on centennial timescales cannot be excluded, The Cryosphere, 17, 3761–3783, https://doi.org/10.5194/tc-17-3761-2023, 2023.

Rignot, E., Jacobs, S., Mouginot, J., and Scheuchl, B.: Ice-shelf melting around Antarctica, Science, 341, 266–270, 925 https://doi.org/10.1126/science.123579, 2013.

Rignot, E., Mouginot, J., Morlighem, M., Seroussi, H., and Scheuchl, B.: Widespread, rapid grounding line retreat of Pine Island, Thwaites, Smith, and Kohler glaciers, West Antarctica, from 1992 to 2011, Geophys. Res. Lett., 41, 3502–3509, https://doi.org/10.1002/2014GL060140, 2014a.

Rignot, E., Mouginot, J., and Scheuchl, B.: MEaSUREs InSAR-Based Ice Velocity of the Amundsen Sea Embayment, Antarctica, Version 930 1, https://doi.org/10.5067/MEASURES/CRYOSPHERE/nsidc-0545.001, 2014b.

Rignot, E., Mouginot, J., Scheuchl, B., van den Broeke, M., van Wessem, M. J., and Morlighem, M.: Four decades of Antarctic Ice Sheet mass balance from 1979–2017, Proceedings of the National Academy of Sciences, 116, 1095–1103, https://doi.org/10.1073/pnas.1812883116, 2019.

Rohardt, G.: Physical oceanography during POLARSTERN cruise ANT-XXII/3, https://doi.org/10.1594/PANGAEA.733664, 2010.

935 Rohardt, G.: Physical oceanography during POLARSTERN cruise ANT-XXIX/2, https://doi.org/10.1594/PANGAEA.817255, 2013.

Rohardt, G. and Boebel, O.: Physical oceanography during POLARSTERN cruise PS103 (ANT-XXXII/2), https://doi.org/10.1594/PANGAEA.881076, 2017.

Rohardt, G. and Boebel, O.: Physical oceanography during POLARSTERN cruise PS117, https://doi.org/10.1594/PANGAEA.910663, 2020.

Rohardt, G., Fahrbach, E., and Wisotzki, A.: Physical oceanography during POLARSTERN cruise ANT-XXVII/2, 940 https://doi.org/10.1594/PANGAEA.772244, 2011.

Ryan, S., Hellmer, H. H., Janout, M., Darelius, E., Vignes, L., and Schröder, M.: Exceptionally warm and prolonged flow of Warm Deep Water toward the Filchner-Ronne Ice Shelf in 2017, Geophysical Research Letters, 47, https://doi.org/10.1029/2020GL088119, 2020.

Scheuchl, B., Mouginot, J., Rignot, E., Morlighem, M., and Khazendar, A.: Grounding line retreat of Pope, Smith, and Kohler Glaciers, West Antarctica, measured with Sentinel-1a radar interferometry data, Geophysical Research Letters, 43, 8572–8579, 945 https://doi.org/10.1002/2016GL069287, 2016.

Schröder, M.: Physical oceanography during POLARSTERN cruise ANT-XII/3, https://doi.org/10.1594/PANGAEA.742581, 2010.

Schröder, M. and Wisotzki, A.: Physical oceanography during POLARSTERN cruise PS82 (ANT-XXIX/9), https://doi.org/10.1594/PANGAEA.833299, 2014.

Schröder, M., Ryan, S., and Wisotzki, A.: Physical oceanography during POLARSTERN cruise PS96 (ANT-XXXI/2 FROSN), 950 https://doi.org/10.1594/PANGAEA.859040, 2016.

Schröder, M., Ryan, S., and Wisotzki, A.: Physical oceanography and current meter data from mooring AWI252-1, https://doi.org/10.1594/PANGAEA.875931, 2017a.

Schröder, M., Ryan, S., and Wisotzki, A.: Physical oceanography and current meter data from mooring AWI253-1, https://doi.org/10.1594/PANGAEA.875932, 2017b.

955 Schröder, M., Ryan, S., and Wisotzki, A.: Physical oceanography and current meter data from mooring AWI254-1, https://doi.org/10.1594/PANGAEA.875933, 2017c.

Schröder, M., Ryan, S., and Wisotzki, A.: Physical oceanography and current meter data from mooring AWI252-2, https://doi.org/10.1594/PANGAEA.903104, 2019a.

Schröder, M., Ryan, S., and Wisotzki, A.: Physical oceanography and current meter data from mooring AWI253-2, https://doi.org/10.1594/PANGAEA.903315, 2019b.

Schröder, M., Ryan, S., and Wisotzki, A.: Physical oceanography and current meter data from mooring AWI254-2, https://doi.org/10.1594/PANGAEA.903317, 2019c.

Seroussi, H., Nakayama, Y., Larour, E., Menemenlis, D., Morlighem, M., Rignot, E., and Khazendar, A.: Continued retreat of Thwaites Glacier, West Antarctica, controlled by bed topography and ocean circulation, Geophys. Res. Lett., 44, 6191–6199, https://doi.org/10.1002/2017GL072910, 2017.

Seroussi, H., Nowicki, S., Payne, A. J., Goelzer, H., Lipscomb, W. H., Abe-Ouchi, A., Agosta, C., Albrecht, T., Asay-Davis, X., Barthel, A., et al.: ISMIP6 Antarctica: a multi-model ensemble of the Antarctic ice sheet evolution over the 21st century, The Cryosphere, 14, 3033–3070, https://doi.org/10.5194/tc-14-3033-2020, 2020.

Seroussi, H., Verjans, V., Nowicki, S., Payne, A. J., Goelzer, H., Lipscomb, W. H., Abe Ouchi, A., Agosta, C., Albrecht, T., Asay-Davis, X., Barthel, A., Calov, R., Cullather, R., Dumas, C., Galton-Fenzi, B. K., Gladstone, R., Golledge, N. R., Gregory, J. M., Greve, R., Hatterman, T., Hoffman, M. J., Humbert, A., Huybrechts, P., Jourdain, N. C., Kleiner, T., Larour, E., Leguy, G. R., Lowry, D. P., Little, C. M., Morlighem, M., Pattyn, F., Pelle, T., Price, S. F., Quiquet, A., Reese, R., Schlegel, N.-J., Shepherd, A., Simon, E., Smith, R. S., Straneo, F., Sun, S., Trusel, L. D., Van Breedam, J., Van Katwyk, P., van de Wal, R. S. W., Winkelmann, R., Zhao, C., Zhang, T., and Zwinger, T.: Insights on the vulnerability of Antarctic glaciers from the ISMIP6 ice sheet model ensemble and associated uncertainty, The Cryosphere, https://doi.org/10.5194/tc-2023-109, 2023.

Shean, D. E., Joughin, I. R., Dutrieux, P., Smith, B. E., and Berthier, E.: Ice shelf basal melt rates from a high-resolution digital elevation model (DEM) record for Pine Island Glacier, Antarctica, The Cryosphere, 13, 2633–2656, https://doi.org/10.5194/tc-13-2633-2019, 2019.

Shepherd, A., Ivins, E., Rignot, E., Smith, B., van den Broeke, M., Velicogna, I., Whitehouse, P., Briggs, K., Joughin, I., Krinner, G., Nowicki, S., Payne, T., Scambos, T., Schlegel, N., Geruo, A., Agosta, C., Ahlstrom, A., Bobonis, G., Barletta, V., Blazquez, A., Bonin, J., Csatho, B., Cullather, R., Felikson, D., Fettweis, X., Forsberg, R., Gallée, H., Gardner, A., Gilbert, L., Groh, A., Gunter, B., Edward, H., Harig, C., Helm, V., Horvath, A., Horwath, M., Khan, S., Kjeldsen, K. K., Konrad, H., Langen, P., Lecavalier, B., Loomis, B., Luthcke, S., McMillan, M., Melini, D., Mernild, S., Mohajerani, Y., Moore, P., Mouginot, J., Moyano, G., Muir, A., Nagler, T., Nield, G., Nilsson, J., Noel, B., Otosaka, I., Pattle, M. E., Peltier, W. R., Pie, N., Bietbroek, R., Rott, H., Sandberg-Sorensen, L., Sasgen, I., Save, H., Scheuchl, B., Schrama, E., Schroder, L., Seo, K.-W., Simonsen, S., Slater, T., Spada, G., Sutterley, T., Talpe, M., Tarasov, L., van de Berg, W., van der Wal, W., van Wessem, M., Vishwakarma, B., Wiese, D., and Wouters, B.: Mass balance of the Antarctic Ice Sheet from 1992 to 2017, Nature, 558, 219–222, https://doi.org/10.1038/s41586-018-0179-y, 2018.

Siahaan, A., Smith, R. S., Holland, P. R., Jenkins, A., Gregory, J. M., Lee, V., Mathiot, P., Payne, A. J., Ridley, J. K., and Jones, C. G.: The Antarctic contribution to 21st-century sea-level rise predicted by the UK Earth System Model with an interactive ice sheet, The Cryosphere, 16, 4053–4086, https://doi.org/10.5194/tc-16-4053-2022, 2022.

Smith, R. S., Mathiot, P., Siahaan, A., Lee, V., Cornford, S. L., Gregory, J. M., Payne, A. J., Jenkins, A., Holland, P. R., Ridley, J. K., et al.: Coupling the UK Earth System Model to dynamic models of the Greenland and Antarctic ice sheets, Journal of Advances in Modeling Earth Systems, 13, https://doi.org/10.1029/2021MS002520, 2021.

Swedish Polar Research Secretariat: Oden Southern Ocean 2009/10 - Conductivity-Temperature-Depth (CTD) Data Collected Onboard Ice-breaker Oden during February through March 2010, Tech. rep., Swedish Polar Research, http://snd.gu.se/en/catalogue/dataset/ecds0220-1, 2010.

Thoma, M., Determann, J., Grosfeld, K., Goeller, S., and Hellmer, H. H.: Future sea-level rise due to projected ocean warming beneath the Filchner Ronne Ice Shelf: A coupled model study, Earth & Planet. Sci. Lett., 431, 217–224, https://doi.org/10.1016/j.epsl.2015.09.013, 2015.

Timmermann, R. and Goeller, S.: Response to Filchner–Ronne Ice Shelf cavity warming in a coupled ocean–ice sheet model–Part 1: The ocean perspective, Ocean Science, 13, 765–776, https://doi.org/10.5194/os-13-765-2017, 2017.

Timmermann, R. and Hellmer, H. H.: Southern Ocean warming and increased ice shelf basal melting in the twenty-first and twenty-second centuries based on coupled ice-ocean finite-element modelling, Ocean Dyn., 63, 1011–1026, https://doi.org/10.1007/s10236-013-0642-0, 2013.

Webber, B. G. M., Heywood, K. J., Stevens, D. P., Dutrieux, P., Abrahamsen, E. P., Jenkins, A., Jacobs, S. S., Ha, H. K., Lee, S. H., and Kim, T. W.: Mechanisms driving variability in the ocean forcing of Pine Island Glacier, Nature Communications, 8, 1–8, https://doi.org/10.1038/ncomms14507, 2017.

Wellner, J.: Cruise NBP2002, RVIB Nathaniel B. Palmer, Jan 25 2020 – Mar 08 2020, Tech. rep., United States Antarctic Program, http://doi.org/10.7284/908803, 2020.

Zhao, C., Gladstone, R., Galton-Fenzi, B. K., Gwyther, D., and Hattermann, T.: Evaluation of an emergent feature of sub-shelf melt oscillations from an idealized coupled ice sheet–ocean model using FISOC (v1. 1)–ROMSIceShelf (v1. 0)–Elmer/Ice (v9. 0), Geosci. Model Dev., 15, 5421–5439, https://doi.org/10.5194/gmd-15-5421-2022, 2022.